Journal of Water Process Engineering 69 (2025) 106586

Contents lists available at ScienceDirect

Journal of Water Process Engineering

journal homepage: www.elsevier.com/locate/jwpe

A novel biochar adsorbent for treatment of perfluorooctanoic acid (PFOA) contaminated water: Exploring batch and dynamic adsorption behavior

Malihe Afrooz [a,c], Rahman Zeynali [a], Jafar Soltan [a,c,*], Kerry N. McPhedran [b,c]

[a] Department of Chemical and Biological Engineering, University of Saskatchewan, Saskatoon, Saskatchewan, Canada
[b] Department of Civil, Geological & Environmental Engineering, University of Saskatchewan, Saskatoon, Saskatchewan, Canada
[c] Global Institute for Water Security, University of Saskatchewan, Saskatoon, Saskatchewan, Canada

ARTICLE INFO

Keywords:
Perfluorooctanoic acid (PFOA)
Microwave-assisted pyrolysis (MWP)
Chemisorption
Activated biochar
Chemical treatment
Canola straw

ABSTRACT

Perfluoroalkyl substances (PFAS), like perfluorooctanoic acid (PFOA), are of concern worldwide given they are ubiquitous in the environment. In this study, the treatment of PFOA-contaminated water was assessed using biochar adsorbents produced from raw canola straw (RCS) through chemical activation with H_3PO_4 and $ZnCl_2$ and microwave-assisted pyrolysis (MWP). MWP conditions were evaluated to create optimal H_3PO_4-treated (PBC) and $ZnCl_2$-treated (ZnBC) biochar adsorbents with treatments determined using a central composite design (CCD) based on the response surface methodology (RSM) considering activator concentration, and microwave heating time and power. The highest PFOA removal efficiency for PBC (3.0 mol/L) was achieved at 92 % (368 μg/g), while for ZnBC (0.55 mol/L) it was 84 % (336 μg/g). In contrast, untreated biochar and RCS had markedly lower PFOA removals of 5 % and 1 %, respectively. Activation of biochar under optimal pyrolysis conditions (6 min at 600 W) led to increased chemical functional groups, porosity, and surface area, as confirmed by FT-IR, XPS, and BET. The kinetic study indicated that chemisorption was the primary PFOA adsorption mechanism, while the Freundlich isotherm model suggested heterogeneous multilayer adsorption for PFOA removal. Further, background salts enhanced PFOA adsorption through divalent bridges and salting-out mechanisms. PBC and ZnBC adsorbents performed well over a broad pH range of 3 to 9. Lastly, Yan and Yoon-Nelson models were used to assess adsorption breakthrough for a model fixed-bed adsorption system. This study exhibits that PBC and ZnBC adsorbents, derived from accessible biomass, offer an environmentally friendly solution to remove PFOA from contaminated water.

1. Introduction

Over the past few years, there has been widespread concern about the presence of perfluoroalkyl substances (PFAS) throughout the environment including in drinking water and food. For example, PFAS compounds including perfluorooctane sulfonate (PFOS) and perfluorooctanoic acid (PFOA) have been reported in agricultural and urban water wells at concentrations as high as 10,000 ng/L indicating their widespread use and potential for groundwater pollution [1]. Concentrations vary from region to region, with Canada and China samples indicating high concentrations of total PFAS >3200 ng/L [2]. Ruyle et al. [3] reported PFOS and PFOA contamination in groundwater at a former firefighting site in Cape Cod, Massachusetts, USA with a maximum PFOS concentration of 22,000 ng/L. Furthermore, 26 PFASs were found in groundwater, surface water, and landfill leachate samples in China with elevated concentrations (up to 10,000 ng/L) in the leachate from municipal solid waste (MSW), while lower concentrations (below 500 ng/L) were detected in groundwater and surface water [4,5].

PFOA is a dominant type of long-chain PFAS commonly detected in various waterbodies, such as wastewater, drinking water, and seawater [6]. For example, in a groundwater sample collected in Europe, PFOA accounted for 48 % of the total number of PFAS compounds identified [7]. Although PFOA has been used for many decades, concerns about its toxicity arose in the early 2000s. For instance, in 2009 the United States Environmental Protection Agency (USEPA) categorized it as potentially carcinogenic [8]. Since 2016, health advisory levels (HALs) have been issued by the USEPA for drinking water with concentrations between 100 and 7000 ng/L for short-chain PFAS compounds (C4–C7) and 70 ng/L for PFOA. Additionally, the Guidelines for Canadian Drinking Water Quality indicate that the maximum acceptable concentration (MAC) is

* Corresponding author at: Department of Chemical and Biological Engineering, University of Saskatchewan, Saskatoon, Saskatchewan, Canada.
E-mail address: j.soltan@usask.ca (J. Soltan).

https://doi.org/10.1016/j.jwpe.2024.106586
Received 11 October 2024; Received in revised form 12 November 2024; Accepted 14 November 2024
Available online 22 November 2024
2214-7144/Crown Copyright © 2024 Published by Elsevier Ltd. This is an open access article under the CC BY license (http://creativecommons.org/licenses/by/4.0/).

0.2 μg/L for PFOA [9]. Thus, PFOA contamination has become a worldwide concern with many researchers investigating its treatment, with a focus on drinking water and wastewater matrices.

The low MAC for PFAS leads to challenges not only for analytical detection methods but also for remediation technologies. Various destructive or non-destructive treatment methods for contaminated waters are available such as advanced oxidation processes (AOPs), defluorination treatment, non-thermal and thermal degradation, and adsorption [10–13]. Current PFAS treatment methods have several limitations, including the generation of secondary waste, incomplete removal of contaminants, and high costs. In addition, traditional treatment methods, such as coagulation and chlorination, are ineffective, and evolving regulations adapt to a slow and costly process [14]. As a result of these challenges, more effective, affordable, and sustainable solutions are required. Adsorption is considered to be a promising, cost-effective method to remove PFAS and has recently been a focus of studies aiming to eliminate various PFAS compounds from water [15]. However, the effectiveness of adsorbents varies based on their properties, the types of targeted PFAS compounds, and the treatment conditions. For example, polar adsorbents can bind with the PFAS molecules through electrochemical interactions with their polar chemical functional groups, while alkyl/aromatic parts of the adsorbent interact with the non-polar parts of PFAS molecules via hydrophobic interaction [16]. Overall, carbon-based substances and their composites have been effectively utilized to remove short-chain PFAS compounds (e.g., PFBA, PFBS, PFH_xA, PFH_xS, and PFPeA,) and long-chain PFAS compounds (i.e., PFOS and PFOA) from water [17].

Carbon-based materials including carbon nanotubes (CNTs), activated carbon (AC), graphene, and biochar are among those proposed as potential adsorbent media for use in treating aqueous phases containing PFAS [18]. AC has been the most used material in both laboratory and field settings for remediating PFAS contaminants [19]. CNTs are hydrophobic, hollow, and one-dimensional structures with large specific surfaces, high adsorption capacity, and high thermal and chemical stabilities. The adaptability of changing 2D nanomaterials is used for the tailoring of graphene toward addressing specific PFAS compounds [20]. However, engineered and low-cost biochar adsorbents can be a promising alternative to other commonly used carbon-based adsorbents in large-scale water treatment because they are eco-friendly, cheaper, and more readily available via common biomasses. For example, biochar requires a lower energy input and releases less greenhouse gasses than AC suggesting that biochar can be a more sustainable option in many applications. Biochar production needs an average energy demand of about 6.1 MJ/kg and has a greenhouse gas (GHG) emission rate of 0.9 kg CO_2/kg, whereas, for AC production, these values were markedly higher, with an average energy demand of 97 MJ/kg and GHG emission of 6.6 kg CO_2/kg [21]. Overall, engineered biochar is a promising option for PFAS treatment; however, further research is needed to assess and improve its adsorption performance.

Historically, conventional furnace pyrolysis has been used for the creation of biochar, however, recent studies have considered microwave-assisted pyrolysis (MWP) as a promising alternative method. Faster reaction rates can be accomplished using MWP given it is selective, volumetric, and uniform, while providing for homogeneous heating and higher heating rates resulting in increased energy efficiency [22]. Generally, the pyrolysis conditions play a crucial role in determining the physicochemical properties of biochar, as organic compounds in biochar break down and convert into new chemicals at different temperatures [23]. Besides pyrolysis conditions, the chemical treatment of biochar (or biomass) can significantly enhance its adsorption effectiveness. This includes treatments with alkaline or acid solutions, as well as the addition of oxidizing agents and metal salts. Generally, these modifications improve the biochar's pore volume, surface area, surface charges, and chemical functional groups [24]. Biochar can be pretreated before pyrolysis or post-treated after this process using various chemical activators, such as acids, bases, and salts. Among these, H_3PO_4, $ZnCl_2$, NaOH, $KMnO_4$, $FeCl_3$, and KOH have proven to be the most effective in increasing adsorption effectiveness [25]. The acid treatment increases surface area, porosity, and chemical functional groups of biochar, providing more potential active sites for binding PFAS molecules vs. untreated biochar.

A major benefit of biochar is that the feedstock biomass can be sourced from waste materials, aligning with circular economy and waste reduction principles. Its unique properties, wide range of uses, low production cost, and promising growth potential highlight its ability to contribute to achieving Sustainable Development Goals (SDGs). Canola straw (CS) is a common agricultural residue in Canada, with an annual production of 14.7 million metric tons. Approximately 60 % of this CS residue is used for animal feed and soil improvement, leaving about 6.0 million metric tons available for other purposes [79]. Therefore, the current study used CS for biochar production due to its availability in Saskatchewan, Canada.

This study offers a novel biochar adsorbent derived from canola straw, activated with H_3PO_4 and $ZnCl_2$ through MWP to remove PFAS compounds. The method improves the biochar properties (surface area, porosity, and functional groups of biochar), leading to higher PFAS adsorption efficiency. The focus of this research was to apply optimized microwave heating and pre-treatment processes to create an effective, novel biochar using RCS for adsorbing PFOA from water. Factors considered in the pre-treatment and pyrolysis processes included activator concentration (mol/L), microwave heating time (min), and microwave power (W). Additionally, the effects of contact time, temperature, pH, ionic strength, and co-existing ions on PFAS adsorption were studied to assess the interactions between PFOA and biochar. Various adsorption isotherm and kinetic models, along with the characterization of the biochar's chemical structure, were applied to explore the adsorption mechanisms of the treated biochar. Furthermore, the efficiency of PFOA removal was assessed using a fixed-bed column system with optimized biochar adsorbents to determine the potential for scaling up the treatment process in the future.

2. Experimental

2.1. Materials

Ortho-phosphoric acid (85 %), zinc chloride ($ZnCl_2$, anhydrous, +98 %), and perfluorooctanoic acid (PFOA) (96 %) were obtained from Thermo Fisher Scientific Inc. (Ontario, Canada). Other chemicals of analytical grade were purchased from Sigma-Aldrich (USA). Millipore deionized (DI) water (Q-H_2O, Millipore Corp) was used for all solutions. Raw canola straw (RCS) was sourced from a farm near Saskatoon, Canada. In the laboratory, the straw was washed with DI water twice and then dried at 70 °C for 24 h. Subsequently, the harvested dried biomass was ground and sieved to produce particles in a size range of 400–840 μm for use in all experiments considered herein.

2.2. Preparation of biochar

Untreated biochar (UBC) was prepared under the optimum MWP condition (see below) without the addition of any activator agents. The activated biochar adsorbents were synthesized by mixing 5 g of RCS with 100 mL of various concentrations of H_3PO_4 and $ZnCl_2$, followed by stirring for 4 h to obtain H_3PO_4-treated biochar (PBC) and $ZnCl_2$-treated biochar (ZnBC) [26]. The final biochar was washed repeatedly with hot and cold water to remove impurities and residual chemicals and dried at 105 °C for 24 h.

Three key synthesis parameters were studied and optimized using a three-factor Central Composite Design (CCD) method based on Response Surface Methodology (RSM). These parameters were activator concentration (X_1; H_3PO_4: 1–5 mol/L, $ZnCl_2$: 0.1–1 mol/L), microwave irradiation time (X_2; 3–9 min), and microwave power (X_3; 300–900 W). Tables S2 and S3 present the detailed experimental design and results for

the experimental and predicted PFOA removal efficiencies for PBC and ZnBC. The center point was repeated six times to assess the reproducibility of the data based on the CCD methodology.

2.3. Adsorbent characterization

The element distribution and surface morphology of adsorbents were investigated by a scanning electron microscope (SEM, Hitachi SU8010, Japan) equipped with an energy dispersive spectrometer (EDS). Under high vacuum conditions, analyses were carried out with a voltage of 5 kV and an emission current of 10 μA. A Brunauer-Emmett-Teller (BET) N_2 analyzer at 77 K (NOVAtouch; Quantachrome, USA) was used to compare the specific surface area, average pore diameter, and total volume of adsorbents. Prior to BET analysis, samples were degassed at different temperatures (60 °C for biomass and 160 °C for biochar). A Bruker X-ray diffractometer (Rigaku Americas Corp., USA) with a scanning speed of 2°/min was used to examine the effects of activators on the crystalline structure of the samples. The Fourier-transform infrared (FT-IR) spectra were recorded by a Smith's Detection IlluminatIR FT-IR microscope (USA) to assess the chemical functional groups of adsorbents. A Renishaw spectrometer (Gloucestershire, UK) was used to provide the Raman spectra of the adsorbents to study the effect of pyrolysis and chemical treatment on the biochar structure. The chemical functional groups and chemical states of elements on the surface of adsorbents were investigated by X-Ray Photoelectron Spectroscopy (XPS) (Kratos Analytical Ltd., UK).

A 1290 Infinity II HPLC system, coupled with a 6470 A triple quadrupole mass spectrometer (HPLC-MS/MS), was used to measure the PFOA concentrations. For this analysis, 80 μL of each sample was injected into the system, and a C18 column (150 mm × 2.1 mm, 3.5 μm) was used (Waters, Milford, MI), operating at a flow rate of 0.5 mL/min. The mobile phase was a mixture of 5 mM ammonium acetate in water and 5 mM ammonium acetate in methanol (50:50). The limitation of HPLC-MS/MS was 1 μg/L for PFOA.

Experimental design calculations were done by Minitab software version 19.0 (Minitab Inc., Pennsylvania, USA). The model equations and subsequent numerical simulations were solved using a commercial CFD package, COMSOL Multiphysics 6.0. The model equations were solved using the finite element method in a two-dimensional Computational Fluid Dynamics (CFD) configuration.

2.4. PFOA adsorption experiments

2.4.1. Batch experiment

Batch adsorption experiments were conducted under various conditions to study the adsorption mechanism (s). The impacts of key adsorption parameters that were examined included: PFOA concentration, adsorbent dosage, pH, temperature, presence of co-existing ions, and ionic strength. The experiments were done in glass bottles containing the corresponding adsorbent dosage and 80 mL PFOA solution, with continuous shaking at 200 rpm on a shaker table. Based on preliminary experiments, 10 h was determined as an appropriate equilibrium time for PFOA adsorption by treated adsorbents. Preliminary batch experiments were carried out with different concentrations of PFOA (100, 200, 500, 1000, and 10,000 μg/L) at various adsorbent dosages (0.25, 0.50, 1.00, and 1.25 g/L) at 25 °C for 24 h to determine the optimum adsorbent dosage. These preliminary experiments were done given that as PFOA concentration increases, the PFOA adsorption efficiency decreases because adsorbents become saturated by PFOA.

A kinetic study of batch adsorption for PBC and ZnBC was performed with a PFOA concentration of 200 μg/L and an adsorbent dosage of 0.5 g/L at 25 °C. Kinetic data was calculated by fitting the experimental results to conventional kinetic models (Table 1). Isotherm experiments were conducted with a PFOA concentration range of 50 to 300 μg/L. The thermodynamic parameters of PFOA adsorption were evaluated at various temperatures of 281, 288, 298, and 308 K. The pH drift method was utilized to obtain the point of zero charge (pH_{pzc}) for PBC and ZnBC. In this method, 40 mg of adsorbent was added to 80 mL of NaCl solution with a pH range of 2 to 13, adjusted by 0.1 M and 1 M HCl and NaOH.

Table 1
Kinetic and isotherm data for PFOA adsorption using PBC and ZnBC.

Model	Equation	Parameter	PBC	ZnBC
Kinetic				
Pseudo-first order	$q_t = q_e(1 - e^{-k_{pfo}t})$	k_{pfo} (1/h)	0.307	0.230
		q_e exp. (μg/g)	368	336
			378	329
		q_e *cal.* (μg/g)	0.922	0.929
		R^2		
Pseudo-second order	$\frac{t}{q_t} = \frac{1}{k_{pso}q_e^2} + \left(\frac{1}{q_e}\right)t$	k_{pso} (g/μg.h)	0.0011	$8.87*10^{-4}$
		q_e *cal.* (μg/g)	408	2.39
		R^2	0.995	0.960
Intra-particle diffusion	$q_t = k_p t^{1/2} + C$	k_p (μg/g.$h^{0.5}$)	40.2	36.9
			124.6	88.1
		C (μg/g)	0.637	0.684
		R^2		
Elovich	$q_t = \frac{1}{b}ln(1 + abt)$	a (μg/g.h)	833	342
		b (g/μg)	0.0162	0.0163
		R^2	0.851	0.838
Isotherm				
Langmuir	$q_e = \frac{K_L q_{max} C_e}{1 + K_L C_e}$	q_{max} (μg/g)	341	317
		K_L (L/μg)	0.164	0.156
		R^2	0.932	0.921
Freundlich	$q_e = K_F C_e^{\frac{1}{n}}$	K_F (μg/g)	121	133
		n	4.53	5.59
		R^2	0.990	0.965
Temkin	$q_e = \frac{RT}{b_T}ln(K_T C_e)$	K_T (L/μg)	13.2	12.1
		b_T (J/mol)	55.0	58.7
		R^2	0.988	0.981

The influence of the initial pH on the adsorption of PFOA from water was analyzed at varying pH range of 3 to 12, and pH adjustments were done using 0.1 M and 1 M HCl and NaOH solutions. Furthermore, different salts (NaCl, Na_2NO_3, Na_3PO_4, Na_2SO_4, and Na_2CO_3 for anions, and KCl, NaCl, $CaCl_2$, and $MgCl_2$ for cations) were added to the water separately to investigate the impact of the co-existing ions on PFOA adsorption. The impact of ionic strength was also studied by adding adsorbent to a solution containing 200 μg/L of PFOA and NaCl at different concentrations of 0, 0.001, 0.01, and 0.1 M.

2.4.2. Fixed-bed adsorption

The fixed-bed adsorption experiments were conducted using a column with an internal diameter of 10 mm. The column was packed with glass beads at the top and bottom, and 0.5 g of adsorbent was packed into the middle section with a height of 5 cm. A solution containing 200 μg/L of PFOA was pumped into the column at a constant upward flow rate of 1.5 mL/min. In order to investigate the dynamic adsorption of PFOA on the adsorbents, two mathematical models were used [27]:

$$\text{Yan model}: \frac{C_t}{C_0} = 1 - \frac{1}{1 + \left(\frac{Vt}{b_Y}\right)^{a_Y}} \quad (1)$$

$$\text{Yoon Nelson model}: \frac{C_t}{C_0} = \frac{exp(a_{YN}t - a_{YN}b_{YN})}{(1 + exp(a_{YN}t - a_{YN}\,b_{YN})} \quad (2)$$

In these equations, t indicates time (min), C_0 is the influent PFOA concentration (μg/L), C_t denotes the effluent PFOA concentration at time t (μg/L), V is the flow rate (mL/min), a_Y and b_Y are the Yan model constants. Yoon- Nelson model constants are shown by a_{YN} and b_{YN}.

2.5. CFD model development

CFD simulations were studied to model the PFOA adsorption in the fixed-bed columns containing PBC and ZnBC adsorbents. The

performance of these adsorption columns was modeled under isothermal and time-dependent conditions, with full details presented in the Supporting Information. Experimental data and models were used to assess the adsorption behavior and breakthrough curves. A grid independence test identified 1,200,000 mesh elements as the optimal grid density, ensuring reliable simulation results. The physical properties, such as density, were constant, and there was no mass transfer resistance between the bulk liquid and the adsorbent.

The CFD model analysis utilized three fundamental equations: continuity, species adsorption kinetics, and momentum balance. These equations were applied to a column setup divided into three sections, allowing for precise modeling of mass transport and adsorption phenomena. The three-dimensional geometry of the columns, illustrated in Fig. S1a, displays a simple scheme of fixed-bed adsorption column performance for PFOA removal using PBC and ZnBC adsorbents. This comprehensive simulation approach can provide insights into the fluid and adsorbate behavior within the fixed-bed column, contributing to a more detailed understanding of the PFOA adsorption process.

3. Results and discussion

3.1. CCD optimization

The CCD-RSM facilitated the optimization of activation and pyrolysis conditions to achieve the highest PFOA adsorption while maintaining the biochar's structural integrity. The full details of the CCD-RSM analysis are included in the Supporting Information. Adsorbents with maximum adsorption efficiency were produced at the optimum values of X_1 (H_3PO_4 or $ZnCl_2$ (mol/L)), X_2 (min), and X_3 (W), as shown in Table S2.

A prediction model was developed based on the independent variables and experimental data relevant to adsorption and evaluated using analysis of variance (ANOVA) tests (Tables S4 and S5). Additionally, surface plots for PBC (Fig. S2) and ZnBC (Fig. S3) can be used to visualize the impacts of the three independent factors of molarity, time, and duration on the adsorption efficiency. The PFOA adsorption on the PBC was affected by three independent variables in the following order: $X_3 > > X_2 > X_1$, as evidenced in the Pareto chart of standardized effects (Fig. S4a). Similarly, this order for ZnBC was $X_2 > X_3 > > X_1$ (Fig. S4b). Overall, the highest PBC adsorption efficiencies were $\geq$ 87 % ($n = 6$) with the conditions of 3 mol/L, 6 min, and 600 W (Table S3). The highest ZnBC adsorption efficiencies were $\geq$ 79 % (n = 6) with conditions of 0.55 mol/L, 6 min, and 600 W. Further experiments were conducted using activated adsorbents (PBC and ZnBC) produced under optimal treatment and pyrolysis conditions. They were used to study the equilibrium, kinetics, isotherm, and thermodynamic analyses and the effect of important environmental factors (e.g., ionic strength, co-existing ions, and pH) to explore the PFOA adsorption mechanism.

At higher concentrations of activator (X_1), penetration of active sites increases, and the opening process of pores is facilitated. However, excess activator can result in the blocking of the biochar pores by preventing the release of volatile compounds, which can negatively affect the biochar characteristics [25]. Extending the microwave heating duration (X_2) leads to improving the biochar porosity by boosting the biomass devolatilization rate (Y. [28]). Nevertheless, long-term biomass exposure to microwave radiation can destroy or widen pores. Increasing microwave power (X_3) intensifies the activation agent's and biomass's reaction, improving the porosity. However, there is a risk of damaging the pores using high microwave power [29]. Overall, the structure of each biochar should be optimized during the synthesis process to obtain the most effective adsorbent to remove the target contaminant.

3.2. Adsorbent characteristics

The BET results indicated that the surface areas for PBC and ZnBC are 1067 and 982 m^2/g, respectively. In contrast, values were significantly lower for the UBC at 17 m^2/g and RCS at 3 m^2/g. Overall, the chemical treatment of biomass with H_3PO_4 and $ZnCl_2$ led to a significant enhancement in the total pore volume of the final obtained biochar. The total pore volume increased from 0.003 cm^3/g for RCS and 0.031 cm^3/g for UBC to 0.553 cm^3/g and 0.481 cm^3/g for PBC and ZnBC, respectively. Additionally, chemical treatment and pyrolysis reduced the average pore size of activated adsorbents. The average pore sizes for RCS and UBC were 14 nm and 12 nm, respectively, which are higher than those for PBC and ZnBC, at 2.23 nm and 2.39 nm, respectively. The chemical treatment expands existing pores and forms additional pores through the dehydration, oxidation, and reduction reactions of activators, leading to a higher surface area and porosity. Subsequent thermal treatment removes volatile components and creates more pore structure, increasing total pore volume and creating a wider distribution of pore sizes [30]. Biochar with a higher surface area has a greater number of active sites for PFOA adsorption. A higher porous structure is also vital for PFOA adsorption because it provides many pathways for PFOA molecules to attach to the internal surface of biochar [30].

SEM images (Fig. 1) illustrate the impacts of MWP and chemical activation on RCS biomass morphology. A smooth surface is observed for RCS (Figs. $1a_1$ and a_2), while after pyrolysis, the fibers expand, generating macro- and mesopores (Figs. $1b_1$ and b_2) [31]. During the activation and pyrolysis processes, chemical treatment with H_3PO_4 promotes the release of volatile compounds and induces dehydration process, resulting in the formation additional micropores and mesopores (Figs. $1c_1$ and c_2). In crosslinking reactions, H_3PO_4 serves as a dehydration agent, facilitating condensation and cyclization processes, leading to the development of the pores [32]. During activation with H_3PO_4, phosphate links form because this acid interacts with chemical functional groups present in the RCS, resulting in the formation of more pores and structural expansion. In addition, H_3PO_4 treatment leads to the formation of –C–P–C– bonds, which is a linkage within the pyrophosphates structure, enhancing the structural stability of the carbon framework [33].

In the case of ZnBC, activation with $ZnCl_2$ promotes penetration into lignocellulosic biomass through interaction with cellulose, resulting in the dissolution of organic compounds and the formation of pores (Figs. $1d_1$ and d_2). $ZnCl_2$ facilitates the hydrolysis and swelling of cellulose in biomass, thereby enhancing the porosity and surface area of the final biochar. Furthermore, the penetration of $ZnCl_2$ into lignocellulosic biomass generates more pores within the biomass [25]. The high boiling point of $ZnCl_2$ (732 °C) allows it to remain liquid during carbonization, providing a stable framework that supports the final carbon structure in biochar. This process leads to the melting of biomass fragments and the destruction of cell walls, leading to the formation of a highly porous structure [25]. The SEM images demonstrate a clear difference among RSC, UBC and treated biochar adsorbents. Activated biochar adsorbents (PBC and ZnBC) have a significantly more porous structure with distinct macropores, mesopores, and micropores. Due to chemical activation, treated biochar adsorbents have a greater surface area and pore formation. Consequently, they are more effective as PFOA adsorbents than RCS and UBC [34,35].

Elemental mapping analysis is presented in Fig. 1 for carbon (C; $1a_3$, b_3, c_3, and d_3), oxygen (O; $1a_4$, b_4, c_4, and d_4), phosphorus (P; c_5), and zinc (Zn; d_5). Overall, all elements were uniformly dispersed over the structure of the biochars indicating their potential to be ideal adsorbents for PFOA. In addition, this uniformity contributes to the enhanced adsorption performance of PBC and ZnBC due to the presence of phosphorus and zinc, which create active sites for binding PFOA molecules. The molecular characteristics and elemental composition of the biochar confirm that the type of chemical activation and pyrolysis conditions drastically affect its properties, significantly enhancing PFOA adsorption. According to EDS analysis in Fig. S5, UBC contains more aromatic parts than the other adsorbents resulting in a higher H/C ratio. The presence of phosphorus in PBC and zinc in ZnBC was also confirmed by EDS analysis (Figs. S5c and d). The formation of functional groups, such as phosphate, confirmed by phosphorus in the EDS results, creates active

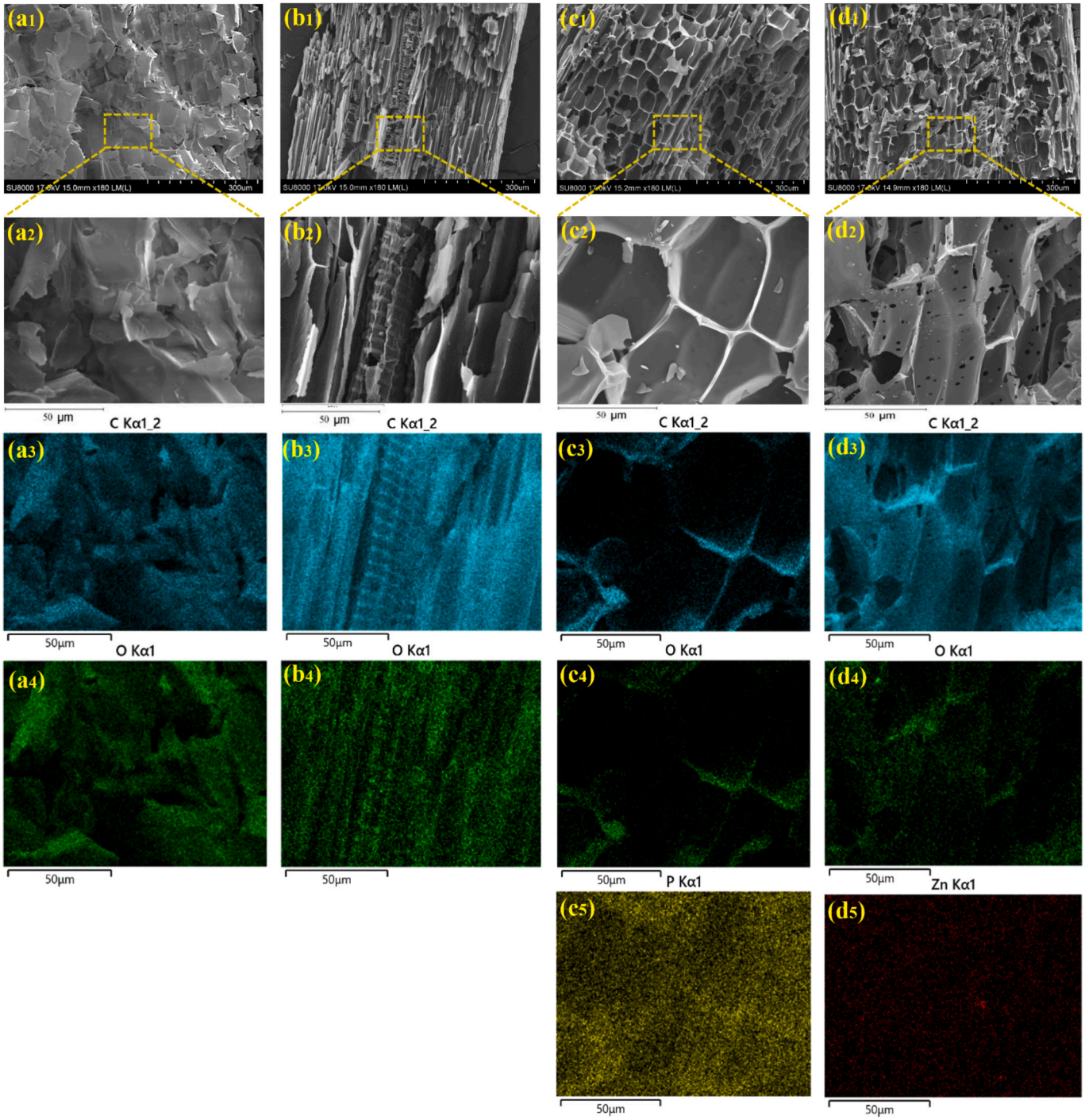

Fig. 1. SEM images (50 and 300 µm) and elemental mapping analysis for: RCS (a_1-a_4); UBC (b_1-b_4; PBC (c_1-c_5); and ZnBC (d_1-d_5).

sites that promote chemical interactions between biochar and PFAS, further enhancing PFOA adsorption. Similarly, EDS analysis of ZnBC confirmed the presence of zinc, indicating the formation of ZnO particles on the biochar. These particles act as active sites for binding PFOA molecules. Furthermore, the higher O/C ratio in PBC reflects more oxygen-containing functional groups, leading to higher hydrophilicity. Therefore, acid groups of PFOA can have more numerous and stronger electrostatic attractions with PBC [36]. This PBC adsorbent contains a greater number of oxygen functional groups than the ZnBC adsorbent.

The XRD pattern of RCS in Fig. 2a revealed that cellulose, hemicellulose, and lignin were all present in canola biomass, associated with three broad diffraction peaks around 15.6, 22.1 and 34.5° [37]. This pattern also shows two types of cellulose (crystalline and amorphous) in RCS. Hemicellulose and lignin are expected to show a broad peak near 16.5° where their amorphous fraction region is located. However, it does not appear in the pattern because of the low intensity and overlapping of peaks [38]. After carbonizing treated samples, XRD patterns show peaks in the 17 to 27° range, indicating graphite structure and the extent of more graphitization of biochar. Moreover, the broad peak that appears between 40° and 48° in PBC is related to the graphitization of biochar with the activation process [39]. The broad peak between 20° and 30° corresponds to the (002) plane of graphite, which is produced using MWP. These crystalline phases make the biochar more robust and effective for adsorption applications [40].

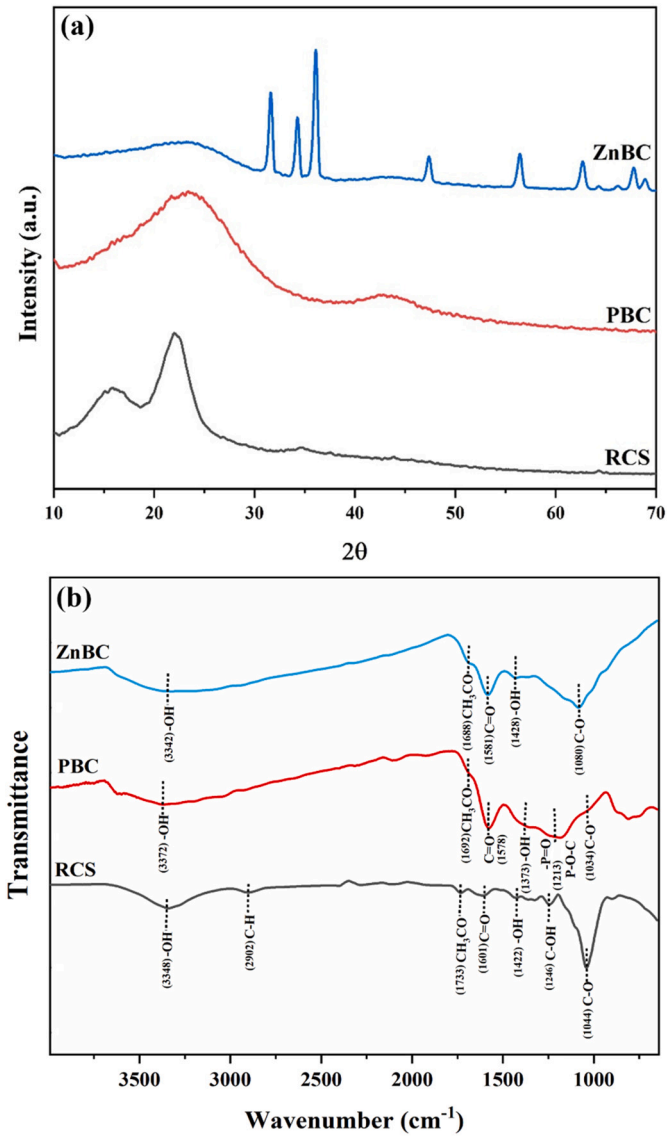

Fig. 2. (a) XRD and (b) FT-IR of RCS, PBC, and ZnBC.

The observed ZnO peaks position for ZnBC has been recorded at 31.6°, 34.3°, 36.1°, 47.3°, 56.4°, 62.7°, 66.2°, 67.8°, and 68.2° as per the Joint Committee on Powder Diffraction Standard JCPDS n° 01–075-0576 [41]. During $ZnCl_2$ activation and pyrolysis, ZnO proceeds through the following reactions [42]:

$$ZnCl_2 + H_2O \rightarrow Zn(OH)Cl + HCl \quad (1)$$

$$Zn(OH)Cl \rightarrow ZnO + HCl \quad (2)$$

In the Raman spectra (Fig. S6), two distinct peaks appeared at 1358 cm^{-1} (D band) and 1590 cm^{-1} (G band) in both PBC and ZnBC. The D band is related to the disordered carbon, whereas the G band is attributable to the graphite structure, suggesting that graphitization takes place during the pyrolysis [43].

FT-IR spectra of the RCS, PBC, and ZnBC exhibit the changes in biochar surface chemistry during the activation and pyrolysis process (Fig. 2b). For RCS, a broad peak around 3300–3500 cm^{-1} can be assigned to the O—H stretching vibrations (carboxyl or alcohol or phenolic -OH). Besides, a second peak around 2900 cm^{-1} shows the C—H stretching of the methyl group. The bands between 1600 and 1700 cm^{-1} can be attributed to C═C bonds in the aromatic ring or C═O bonds in conjugated systems. The peaks in the regions near 1380–1400 cm^{-1} correspond to the phenolic -OH groups or C—O stretch of carboxylate or aliphatic C—H. Another peak at about 1050–1100 cm^{-1} also appears in the spectrum, related to the C-OH stretching peak [44].

In the PBC spectrum (Fig. 2b), there is also a broad band at 1000 to 1400 cm^{-1} with a maximum at 1217 cm^{-1}, which can be ascribed to the oxidized carbons and the carbons induced with phosphoric acid [45]. Phosphorus and phosphocarbonaceous have also absorption in this region. A band at 1203 cm^{-1} can be related to the phosphoric ester compounds. The overlapping of absorption bands from oxygen and phosphorus functional groups in this region complicates the labeling of the bands. However, the resonance absorption in the range of 1000–1300 cm^{-1} range explains the stretching mode of P═O in phosphate aliphatic esters, O—C stretching in P-O-C (non-aromatic), and groups like P=O(OH) in polyphosphates or phosphates [45]. FT-IR spectra of ZnBC and PBC show some differences associated with the phosphorus functional group present in PBC at 1000–1300 cm^{-1} (Fig. 2b). The FT-IR spectrum of ZnBC indicates changes in peaks compared to RCS, especially in the 2800 to 3800 cm^{-1} and 1000 to 2000 cm^{-1} ranges, due to the loss of some chemical functional groups during the degradation of lignocellulosic matter during chemical treatment and carbonization [46].

The FT-IR results demonstrate that RCS, PBC, and ZnBC undergo significant chemical changes during the chemical treatment and pyrolysis processes. The appearance of new peaks or shifts of the existing peaks in the FT-IR spectra reflects these changes. During the degradation of the RCS, some chemical bonds were broken leading to the reduction or loss of related bands in the FTIR spectra (e.g., C—C, C—H, O—H, C—O, C═O). For example, the hydrogen removal attributed to the activation process occurs at about 2900 cm^{-1}, as indicated by the disappearance of the band at this frequency [47]. The incorporation of phosphorus into the activated samples was confirmed by bands characteristic of phosphates and phosphoric acid esters. Generally, the FT-IR technique supported the initial assumptions and provided additional structural information on biochar changes. Chemical functional groups on biochar, including carboxyl, hydroxyl, and phosphate groups, play a key role in the effectiveness of PFAS adsorption through mechanisms such as electrostatic interactions, covalent bonding, and hydrogen bonding. These groups improve adsorption efficiency by providing active sites that interact with the polar head groups and fluorinated chains of PFOA molecules [48]. As a result, the adsorption capacity of PFOA for various adsorbents could be related to their special surface chemistry and different chemical interactions of adsorbent with adsorbate.

XPS analysis of UBC, PBC, and ZnBC was carried out to determine the surface elemental bonds and composition of each adsorbent (Fig. 3). The XPS spectra of adsorbents showed the presence of C, O, P, and Zn elements (Fig. 3a). The F1s peak, corresponding to PFOA adsorbed on PBC and ZnBC, can be seen around 688 eV (Fig. 3b). Spectra of C1s of UBC were qualitatively deconvoluted (Fig. 3c). Four distinct peak locations at 282.12, 282.60, 284.20, and 285.72 eV were found and can be assigned to C—C, C═C, C—O and C═O, respectively [49]. The PBC (Fig. 3d) also presents similar peaks, for instance, at 284.20, 284.39, 285.76, and 287.78 eV, related to C—C, C═C, C—O, and C═O, respectively. In the C1s spectrum of PBC, a peak at 284.80 eV confirms the existence of C—P bonds indicating that the H_3PO_4 activation leads to changes in surface chemistry by incorporating phosphorus. In the case of ZnBC, C—C, C═C, C—O and C═O bonds appear at 284.52, 284.70, 285.99, and 288.70 eV, respectively (Fig. 3e). The O1s spectrum of UBC presented main peaks at 528.82 eV and 529.80 eV, which were identified as C═O and C—O, respectively (Fig. 3f). In the PBC spectrum, the same peaks were placed at 530.61 eV (C=O) and 532.31 eV (C—O), and in ZnBC, at 530.50 eV (C=O) and 531.70 eV (C—O) (Figs. 3g and h). Also, sub-peaks were found in the P2p spectrum of PBC, at 131.94 eV (C-P=O), 133.20 eV (C-P-O), and 133.89 eV (C-O-P) (Fig. 3i).

Two spin orbitals, 1022.06 eV (Zn2p3/2) and 1045.17 eV (Zn2p1/2) can be seen in the Zn2p spectrum of ZnBC (Fig. 3j) (Y. [50]). Fig. 3b

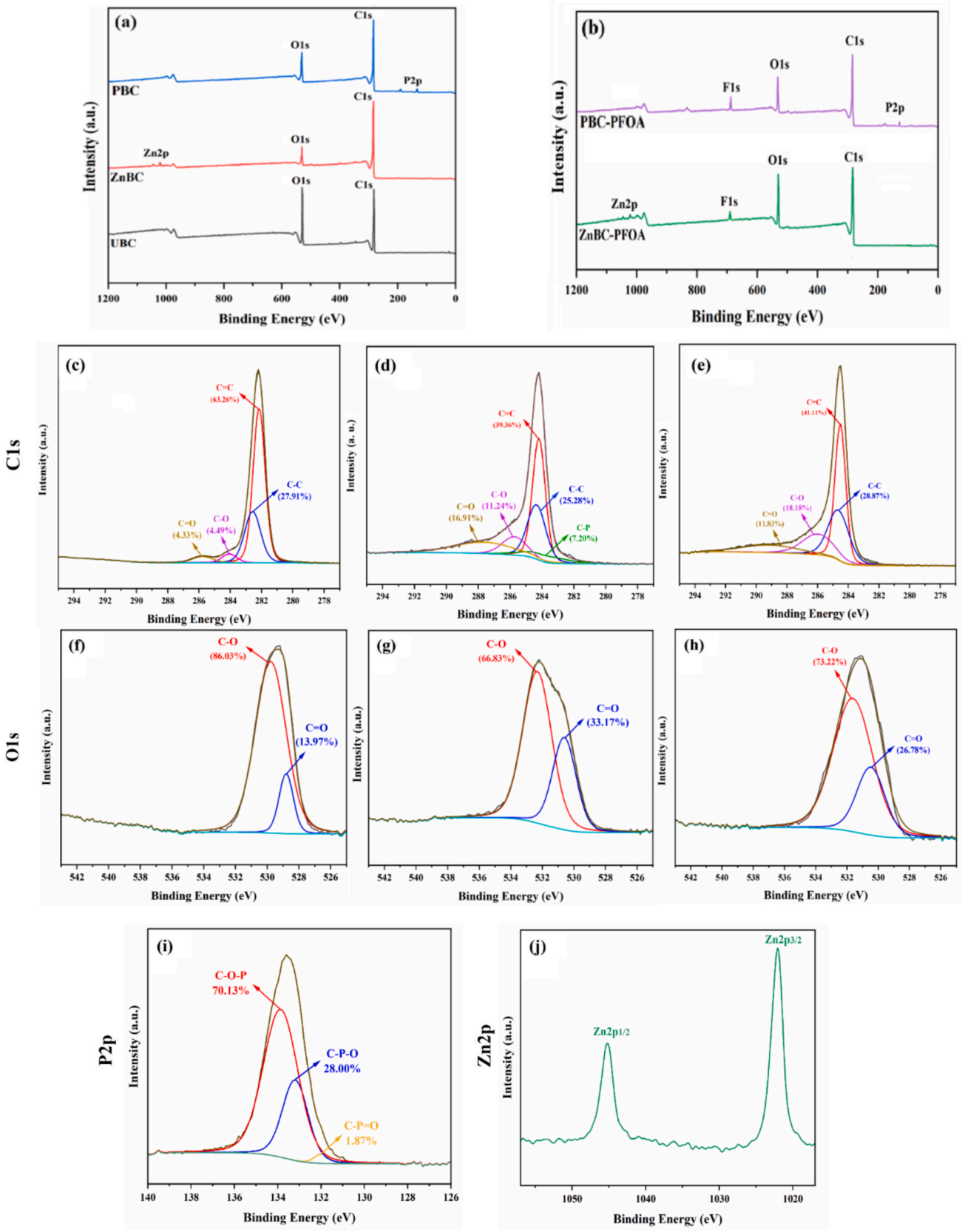

Fig. 3. XPS spectra of (a) UBC, ZnBC, and PBC; and (b) PBC and ZnBC after PFOA adsorption. High-resolution XPS of (c) UBC: C1s, (d) PBC: C1s, (e) ZnBC: C1s, (f) UBC: O1s, (g) PBC: O1s, (h) ZnBC: O1s, (i) PBC: P2p, and (j) ZnBC: Zn2p.

confirms the presence of F on PBC and ZnBC adsorbents after PFOA adsorption. F1s peaks were observed at 688.36 eV and 690.21 eV in PBC and ZnBC spectra (Fig. 3b). After the adsorption of PFOA, the F1s peaks for PBC and ZnBC appeared at 688.36 eV and 690.21 eV, respectively (Fig. 3b) [51]. The treatment of biomass by H_3PO_4 led to phosphorus doping in PBC and enhancing acidic functional groups. As a result, treatment with H_3PO_4 increased the content of C═O functional groups in the C1s spectral area from 4.33 % in UBC to 16.91 % in PBC (Figs. 3c and d), and in the O1s area from 13.97 % in UBC to 33.17 % in PBC (Figs. 3f and g). Likewise, using $ZnCl_2$ increases the amount of C═O functional groups in the C1s area from 4.33 % for UBC to 11.83 % for ZnBC (Figs. 3c and e), and in the O1s area, it goes from 13.97 % for UBC to 26.78 % for ZnBC (Figs. 3f and h).

By sharing electrons between two atoms, covalent bonds are formed; oxidation states are determined by their relative electronegativities. Carbon has a positive oxidation state when it bonds with more electronegative atoms, such as oxygen. In contrast, when carbon is bonded to less electronegative atoms, such as hydrogen or phosphorus, it becomes negative or neutral. Oxygen has an oxidation state of −2 because of its high electronegativity. Phosphorus' oxidation state depends on its chemical environment. There are single (C—C) and double (C=C) bonds in treated adsorbents, where the carbon atoms typically have neutral or slightly reduced oxidation states. In addition to C—O bonds, the treated biochar adsorbents also contain C═O bonds, in which oxygen, as a highly electronegative atom, pulls electron density away from the carbon atoms, resulting in higher oxidation states for carbon [52,53].

3.3. Adsorption kinetic, isotherm, and thermodynamic study

Figs. 4a and b present a high rate of PFOA adsorption with >70 % adsorption efficiency within the first 5 h, before stabilizing within 10 h when adsorption efficiency exceeds 90 %. This indicates that most PFOA molecules diffusing from the liquid medium were rapidly transported to the surface of both PBC and ZnBC through adsorption. The pseudo-second-order model best fits PFOA adsorption on the activated adsorbents with values of $R^2 = 0.995$ and $R^2 = 0.960$, respectively (Table 1).

The kinetic model and mechanism proposed that chemisorption was the rate-controlling step in this study. Therefore, the kinetic results indicate that chemisorption was the most crucial step in the PFOA adsorption process, involving electron exchange and sharing between PFOA and the functional groups of biochar [42]. The higher the initial concentration of PFOA, the greater the experimental adsorption

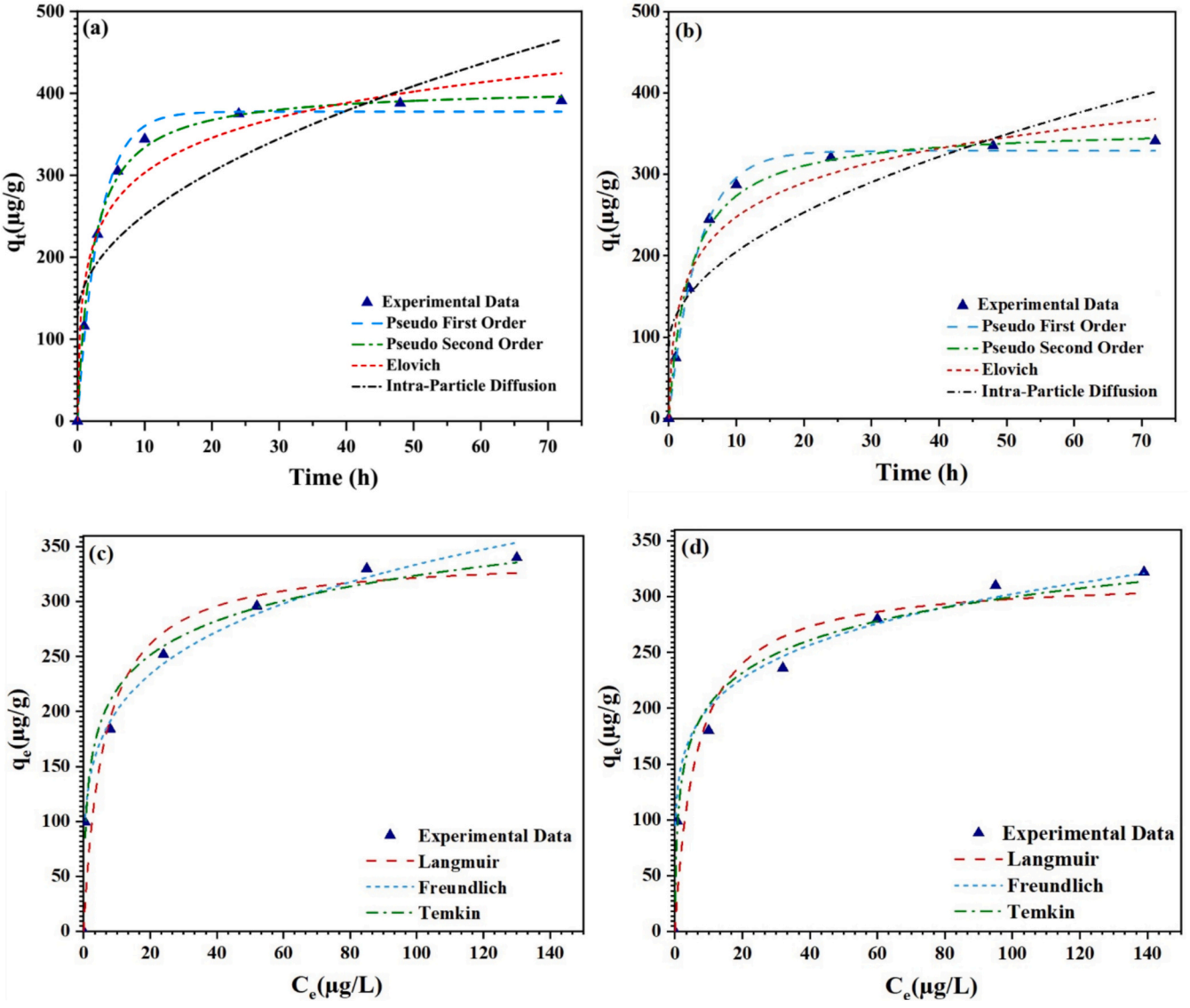

Fig. 4. Sorption kinetics and isotherms of PFOA on PBC (a and c) and ZnBC (b and d) (Note: adsorbent dosage = 0.5 g/L; PFOA initial concentration (kinetic tests) = 200 μg/L; temperature = 25 °C).

capacity, indicating a stronger driving force for adsorption [54]. In addition to the predominant electron-sharing process, other chemical mechanisms, such as electron exchange and surface complexation, have been found to enhance the adsorption of PFOA [55]. Accordingly, Lei et al. reported that PFOA adsorption on mesoporous carbon is more accurately represented by the pseudo-second-order kinetic model [49]. Even in rice straw-derived biochar, PFOS adsorption was best fitted to the pseudo-second-order kinetic model [56].

Kinetic and characterization data indicate that chemical treatment effectively enhanced the quantity of chemical functional groups, porosity, and surface area of the produced biochars. This improvement increased the number of active sites on the biochar structure, thereby enhancing the chemical interactions between PFOA molecules and heteroatoms on the biochar surface. Consequently, these enhancements helped to facilitate the PFOA adsorption and increase the adsorption capacity of the biochar [57](D. Q. [9]).

Adsorption isotherm results were also analyzed to evaluate the interactions between PFOA molecules and both PBC and ZnBC at equilibrium (Figs. 4c and d). The isotherm data for PFAS adsorption were modeled using three different isotherm models: Freundlich, Langmuir, and Temkin. Conducting isotherm adsorption experiments demonstrated that when the PFOA concentration ranged from 50 to 300 μg/L, the PFOA uptake increased from 99 to 340 μg/g. In the case of ZnBC, the adsorption capacity increased from 96 to 322 μg/g. The Freundlich model best fits the experimental data for both adsorbents, with R^2 = 0.990 for PBC and R^2 = 0.965 for ZnBC (Table 1). The Freundlich model indicates that multilayer adsorption occurred for both PBC and ZnBC. This model predicts a heterogeneous adsorbent surface with a non-uniform energy distribution [58]. The diverse chemical functional groups and porosity on the biochar surface led to the formation of multiple adsorption layers for PFAS molecules.

PFOA can interact hydrophobically with mesoporous carbon adsorbents, leading to micelles and a multilayer adsorption process [49]. The PBC had more acid groups and could bind with PFOA molecules more diversely. The multilayer adsorption is also characterized by the hydrophobic interactions that occur between the PFOA molecules (through

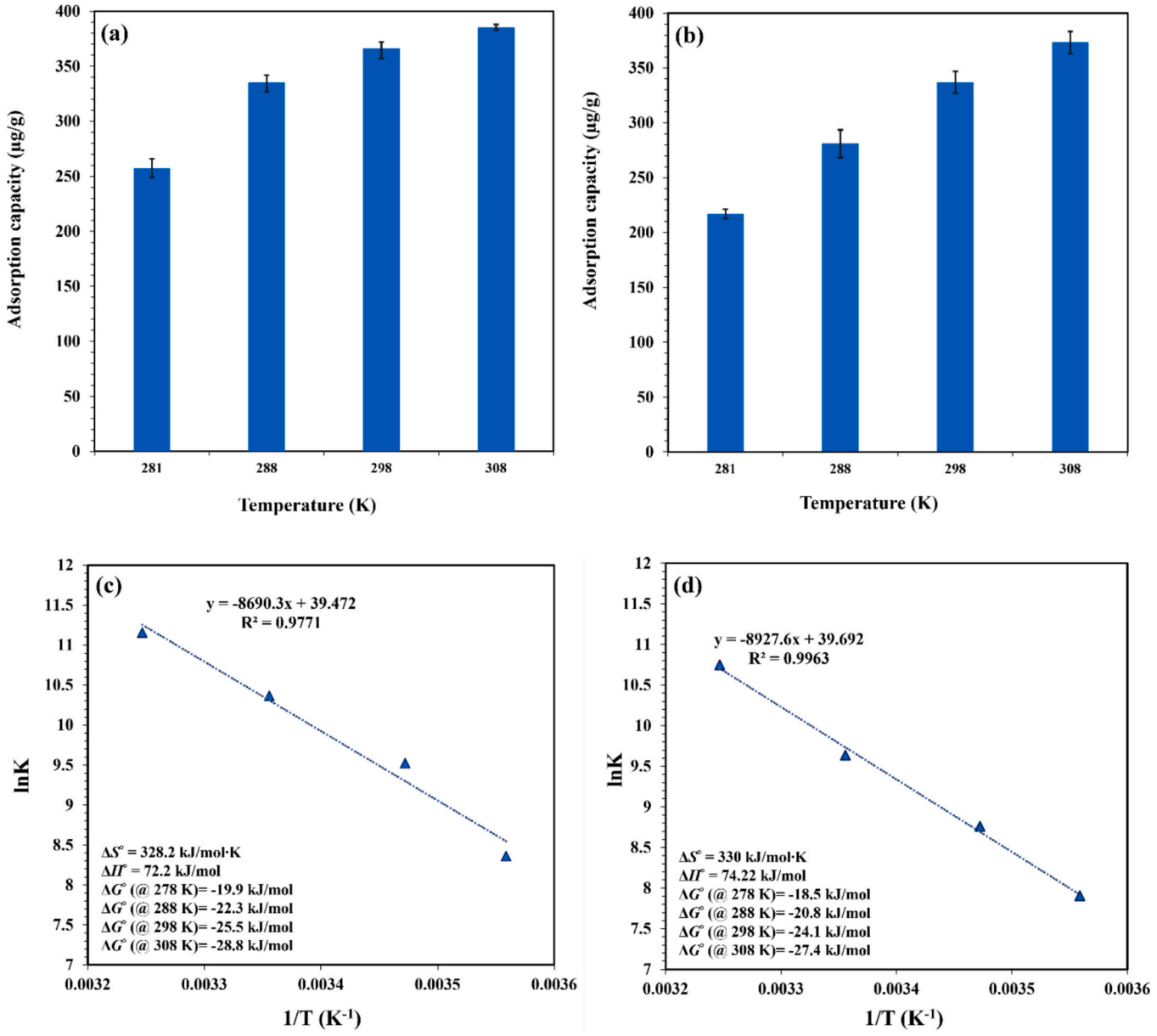

Fig. 5. The effect of temperature on PFOA adsorption capacity for (a) PBC and (b) ZnBC. Thermodynamic parameters for (c) PBC and (d) and ZnBC. (Note: adsorbent dosage = 0.5 g/L; PFOA initial concentration = 200 μg/L; Error bars represent standard deviations with n = 3).

the self-association of hydrophobic parts of PFOA molecules) and the generation of semi-micelles and micelles (W. [59]). In a similar study, the Freundlich model best fit the experimental data for PFOA adsorption on rice straw-based biochar [60]. In addition, Saawarn et al. found that the Freundlich model better represented the isothermal results for PFOA adsorption on magnetic biochar [61].

Overall, the experimental result best fits were found for the Temkin model for PBC and ZnBC (Table 1), confirming that electrostatic interactions predominantly govern the PFOA adsorption on the adsorbents (S. [62]). Zhang et al. found that electrostatic interactions were the primary driving force for the chemical adsorption of PFOS on hydrous ferric oxide and that this process also followed the Temkin model [63]. These interactions occur between the functional groups of the PFOA molecule and the surface of the adsorbent. The amphiphilic nature of PFOA leads to complex aggregations, such as micelles and bilayers, on the adsorbents. Modifying biochar to incorporate phosphorus, zinc, and oxygen functional groups proves more effective in binding PFOA. These strategic improvements result in the formation of more chemical bonds, thereby enhancing PFOA aggregation.

This study investigated the thermodynamic stability of RCS, UBC, PBC, and ZnBC adsorbents. RCS and ZnBC exhibited deficient PFOA adsorption capacities and minimal temperature effects on their adsorption capacities. To obtain a meaningful analysis of thermodynamic parameters, we focused on PBC and ZnBC since they demonstrated significantly higher adsorption capacities. Fig. 5 presents the temperature dependence of the adsorption capacities of PBC and ZnBC adsorbents and the related van t' Hoff derived thermodynamic parameters (ΔH°, ΔG° and ΔS°) of PFOA adsorption [64]. As the temperature increased from 281 to 308 K, PFOA adsorption was significantly enhanced with maximums of 384 μg/g for PBC and 366 μg/g for ZnBC (Figs. 5a and b). Higher temperatures can enhance biochar's adsorption capacity in endothermic adsorption processes [65]. In applications such as wastewater treatment and soil remediation, biochar effectively removes pollutants. The increased kinetic energy of molecules in warmer environments improves biochar's efficiency in adsorbing contaminants [66].

The ΔG° values are negative for both PBC and ZnBC (Figs. 5c and d), which indicates that PFOA adsorption is spontaneous and thermodynamically favorable. The enthalpy values for PBC and ZnBC are 72.20 and 74.22 kJ/mol, respectively, indicating the involvement of

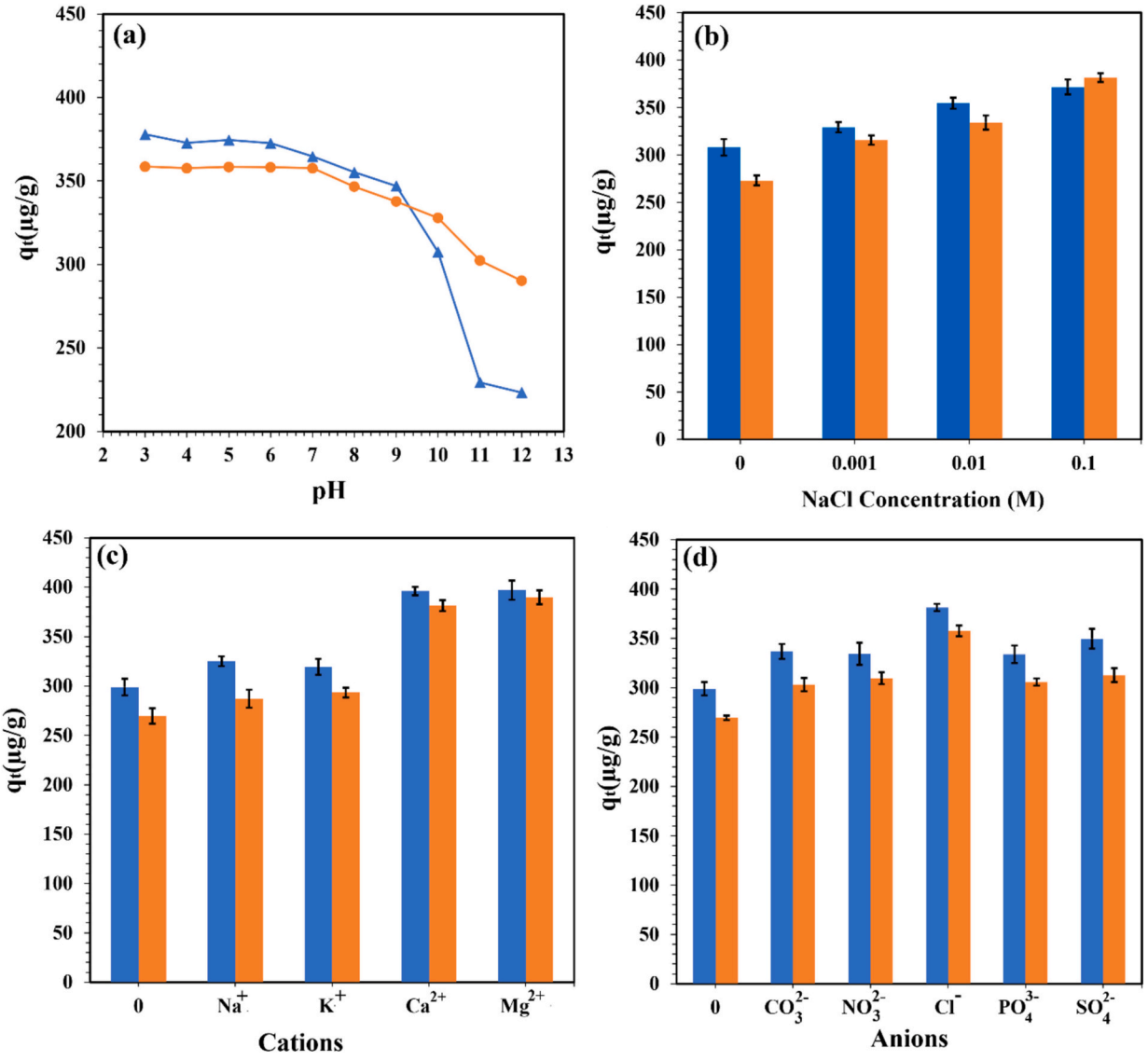

Fig. 6. The effect of (a) pH; (b) ionic strength; (c) cations; and (d) anions on the PFOA adsorption capacity for PBC and ZnBC. (Note: adsorbent dosage = 0.5 g/L; PFOA initial concentration = 200 μg/L; temperature = 25 °C; Error bars represent standard deviations with $n = 3$. Diagrams for PBC are in blue, and ZnBC are in orange). (For interpretation of the references to colour in this figure legend, the reader is referred to the web version of this article.)

chemisorption in the PFOA adsorption process. The positive value of ΔH° confirms the endothermic nature of PFOA adsorption and suggests that primarily chemisorption drives the ΔG° of the adsorption.

PFOA molecules chemically interact with activated adsorbents by breaking weak intermolecular bonds like non-covalent interactions (i.e., van der Waals forces and hydrogen bonds) between biochar and PFOA molecules and forming stronger chemical bonds through electrostatic attractions (dative and ionic bonds). Therefore, PFOA adsorption requires energy input and is endothermic. The positive ΔS° values indicate an increase in system disorder as some adsorbed molecules reoriented or moved on the biochar surface. Enhanced mobility of PFOA molecules on the biochar surface is related to the complex interactions during adsorption, during which structured solvent layers at the interface between adsorbent and solvent are disrupted. The adsorption of PFOA on the biochar surface increases the randomness of the system by disrupting the reorientation of solvent molecules on the surface [67]. The increase in entropy results from the rearrangement of water molecules at the interface of treated biochar adsorbents and PFOA. Moreover, changes in solvation structure and the formation of hydration shells affect the entropy during the adsorption process [68].

3.4. Effects of pH, ionic strength, cations, and anions on PFOA adsorption

Fig. 6a shows the impact of pH changes on the PFOA adsorption process on the PBC and ZnBC adsorbents. As the pH level increased from 7 to 12, PFOA adsorption on ZnBC declined steadily, while for PBC, this decrease was observed as the pH level increased from 8 to 13. Based on the FT-IR results, PBC had more acid groups and, thereby, more positive charges than ZnBC. As a result, PBC had more and stronger electrostatic attraction with PFOA anions and showed higher PFOA adsorption capacity at lower pH levels (3–9). By increasing the pH level of the solution, the PBC surface chemistry changed as well. At high pH values (alkaline conditions), the biochar becomes negatively charged, leading to the electrostatic repulsion forces between the biochar surface and PFOA anions leading to a decrease in the adsorption capacity. The PBC attracted more hydroxide ions at higher pH levels, so it is more influenced by pH than ZnBC [49].

The pH_{pzc} values for ZnBC and PBC were 6.08 and 3.65, respectively. The pK_a value of PFOA is 2.8, thus, it exits primarily in a deprotonated anionic form in most waters [69]. The number of oxygen-containing groups, especially acid functional groups, in ZnBC was lower than in PBC which is in agreement with its higher pH_{PZC}. This implies that the surface chemistry of these adsorbents differed at different pH levels and, therefore, affected the PFOA adsorption. At a pH level less than pH_{pzc}, the adsorbent surface becomes positively charged resulting in the attraction of PFOA anions through electrostatic forces. At pH values higher than pH_{pzc}, the negatively charged adsorbent and PFOA anion will repel each other due to electrostatic interaction, which can negatively affect the adsorption efficiency. In this case, the adsorption of neutral PFOA molecules and cation forms of PFOA (from dissociating a hydrogen ion) on the adsorbent surface is more possible. Moreover, under these conditions, PFOA can be adsorbed through hydrophobic interactions between the alkyl chain or aromatic fractions of the carbon-based adsorbents and the alkyl tail of PFOA (F. [70]).

Fig. 6b illustrates the impacts of ionic strength and different common ions found in water bodies on the PFOA adsorption capacities of PBC and ZnBC. Increasing the ionic strength from 0 to 0.1 M induced the salting-out effect thereby enhancing the hydrophobic interactions between activated adsorbents and the salting-out PFOA leading to improved PFOA adsorption [71,72]. Nevertheless, NaCl has been shown to negatively affect PFOA adsorption given chloride ions (Cl^-) with PFOA for positive sites on the biochar surface. However, PBC and ZnBC have different functional groups leading to variable behaviors at various ionic strengths. PBC had more active sites (functional groups containing P and O), making it more sensitive to changes in ionic strength. At higher ionic strength (0.1 M NaCl), increased competition between Cl^- ions and PFOA occurred resulting in reduced PFOA adsorption and less improvement in PFOA uptake for PBC compared to ZnBC.

The effect of different cations (Fig. 6c) and anions (Fig. 6d) on the PFOA adsorption is presented for treated adsorbents. In this study, the effects of individual ions on PFOA adsorption were investigated instead of using a mixed-ion solution, allowing for a clearer understanding of specific interactions and mechanisms. When single ions are observed, a deeper understanding of adsorption mechanisms can be gained, which is crucial for optimizing an adsorbent for practical use. Divalent cations (Ca^{2+} and Mg^{2+}) significantly enhanced the adsorption efficiency of both PBC and ZnBC. The addition of these cations increases the zeta potential by neutralizing the biochar surface. They can form a complex structure by acting as a bridge between the functional groups of PFOA and the negatively charged regions of the biochar. Wang et al. reported that PFOA and PFOS exhibited a similar adsorption mechanism on alumina adsorbents in the presence of divalent cations (Mg^{2+} and Ca^{2+}) (F. [70]). The salting-out effect also occurs when anions were added to the solution and enhanced the PFOA adsorption (Fig. 6d). In this work, the most common anions found in water solutions like Cl^-, CO_3^{2-}, NO_3^-, PO_4^{3-}, and SO_4^{2-}, were studied. The anion effect on the PFOA adsorption was more observed for smaller anions like Cl^-, resulting in higher adsorption capacity for treated adsorbents [49]. Nevertheless, the anions can compete with PFOA anions to attach to the positive sites on the biochar, which can negatively impact PFOA adsorption. Therefore, the effects of anions on the PFOA adsorption capacity were less than cations.

3.5. Fixed-bed column modeling of PFOA adsorption using PBC and ZnBC

The effectiveness of each adsorbent in a continuous flow system was studied to evaluate their potential for use in a fixed-bed column to remove PFOA from wastewater. Yan and Yoon-Nelson models were used to determine the exhaustion point (t_e), breakthrough point (t_b), and time to 50 % breakthrough (τ) to assess the obtained experimental data for PFOA adsorption (Figs. 7a and b). The t_e was determined as the time at which outlet contaminant concentration reaches 95 % of the influent concentration. The t_b shows when the effluent PFOA concentration achieved 5 % of the influent concentration, and the τ refers to the time required for the adsorbate to reach a 50 % breakthrough [27]. In the Yan model, t_e was calculated at 480 min for PBC, while this amount was 433 min for the Yoon-Nelson model. For ZnBC, this parameter in the Yan model was 378 min, and in the Yoon-Nelson model, it was 335 min. Consequently, PBC was shown to eliminate PFOA for a longer treatment time than ZnBC. The experimental findings show that the value of τ for PBC is 257 min, while it was obtained 244 min and 250 min for the Yan and Yoon-Nelson models, respectively. The experimental value of τ for ZnBC is 178 min, while for the Yan and Yoon-Nelson models, it was 182 and 190 min, respectively. The performance of both the adsorbents was considered to be acceptable in a continuous flow system; however, the PBC held the 50 % breakthrough for a much longer period.

Although there are slight differences in the breakthrough and exhaustion times estimated by the Yan and Yoon-Nelson models, the experimental data align closely with both models ($R^2 \geq 0.98$). The Yan model is generally acknowledged to be an empirical model for predicting breakthrough curves [73]. In contrast, the Yoon-Nelson model predicts that there will be a decline in the probability of adsorption for each adsorbate molecule (PFOA), and this decline is associated with both adsorbate breakthrough and adsorption probability [27]. Although these models predict the adsorption behavior, they ignore some important factors such as intraparticle mass transfer and axial dispersion, which significantly affect the mass transfer dynamics. In this study, a mass transfer model was developed and assessed in order to address these limitations. This model aims to optimize effective diffusion and external mass transfer coefficients simultaneously [74].

As demonstrated in Figs. 7c and d, this model offers a 3D concentration profile within the system at 60, 100, 400, and 500 min for (c) PBC and (d) ZnBC. The potential to use this profile to optimize and

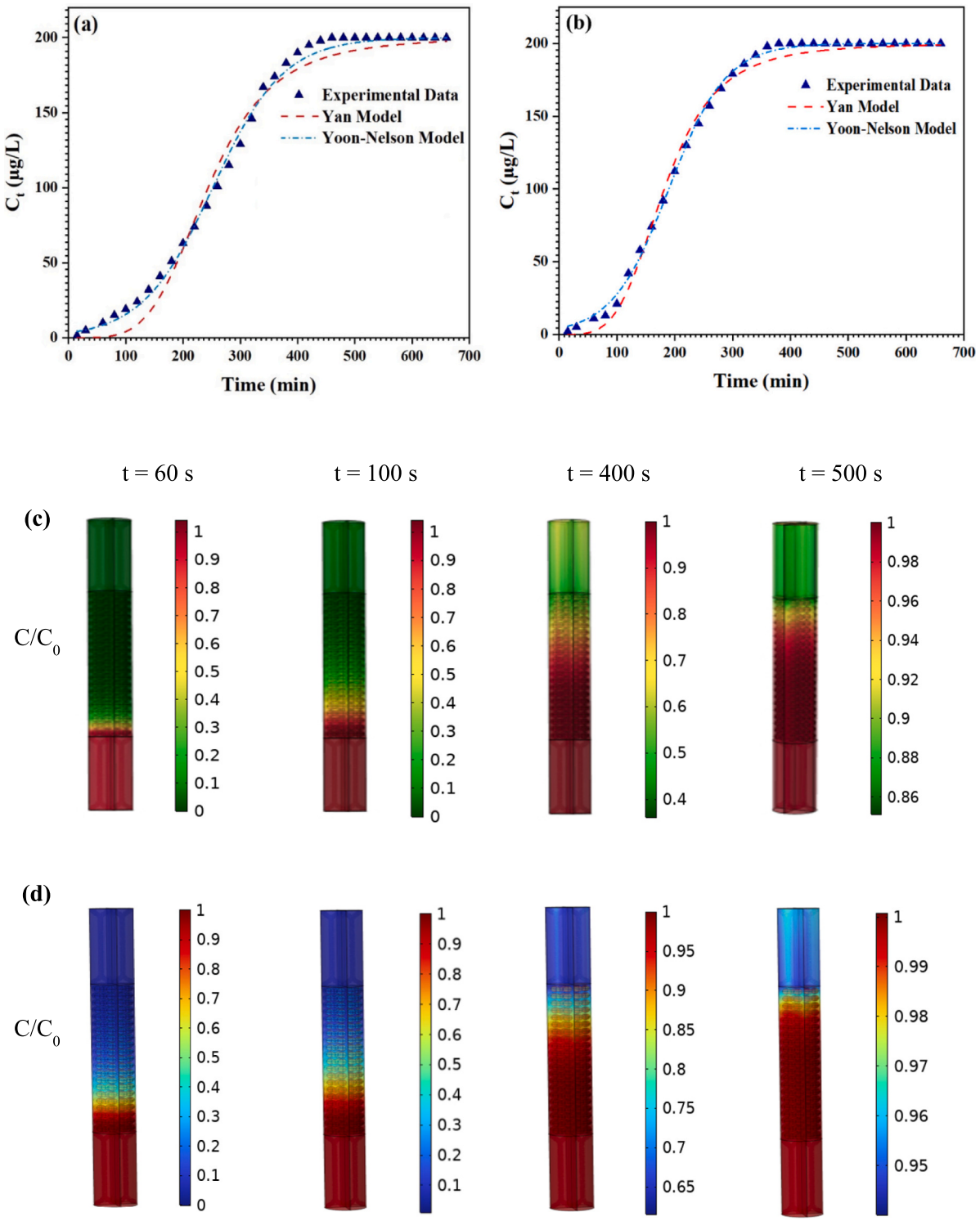

Fig. 7. Modeling of the breakthrough curve for adsorption of PFOA onto (a) PBC and (b) ZnBC using Yan and Yoon-Nelson models. PFOA concentration profile (C/C_0) within the fixed-bed adsorption system at times of 60, 100, 400, and 500 min for (c) PBC, and (d) ZnBC at a bed height of 5 cm.

design a more extensive fixed-bed adsorption system for industrial-scale applications is a promising prospect based on the model and mass transfer coefficients. The PBC column performed better in PFOA adsorption than the ZnBC column. This was due to PBC's surface chemistry and surface area, which was investigated using several analytical approaches such as FT-IR, BET, SEM, and XPS. Therefore, the biochar characteristics influence the parameters t_b, te, and τ. For PBC, t_b, t_e, and τ were 60, 400, and 257 min, respectively, while these parameters were 54.5, 336.5, and 178.6 min for ZnBC, respectively. PBC was more effective than ZnBC at a longer period in flow conditions in low concentrations of PFOA.

3.6. *Possible PFOA adsorption mechanisms on biochar*

Hydrogen bonding, electrostatic attraction, hydrophobic interactions, pore filling, and van der Waals forces are critical in PFOA

adsorption on activated biochars [75]. The use of H_3PO_4 during the pyrolysis process often leads to the loss of volatile substances and water, altering the surface chemistry (chemical functional groups), surface area, and porosity of biochar. This modification arises from the decomposition of organic matter in biomass, which increases micropores and mesopores. The enhanced porosity allows PFOA molecules to diffuse into internal pores, improving retention. BET analysis revealed an increase in the specific surface area of PBC and a rise in pore volume, facilitating PFOA diffusion and retention within the internal pores. SEM images indicate extensive, interconnected porosity, further confirming the high surface area and porosity of the activated biochar adsorbent.

Phosphoric acid interacts with hydroxyl (-OH) groups of lignin, hemicellulose, and cellulose, leading to the formation of phosphorus-containing groups (C—P and C-O-P) on the RCS structure, resulting in a positively charged biochar (Fig. 8a) [76]. Rosas et al. (2008) [80] suggest that the release of CO from phosphoric acid-activated carbons at high temperatures may relate to the cleavage of C-O-PO_3 bonds and the formation of C-PO_3 bonds. Valero-Romero et al. report that phosphorus functional groups enhance adsorbent effectiveness for PFOA binding [77]. The H_3PO_4 activation step promotes the formation of additional -OH and -COOH surface functional groups, which increase the potential for covalent and hydrogen bonds with PFOA, serving as active interaction sites. Oxygen- and phosphorus-containing groups in treated biochar were successfully characterized by EDS, FT-IR, and XPS techniques.

During the activation of H_3PO_4, phosphorus atoms are introduced to the biochar surface, where phosphorus atoms, particularly those on the PBC, have empty *d* orbitals, providing positive sites. A dative bonding occurs between the phosphorus atoms and the carboxylate or carboxylic groups of PFOA, which donate electrons to the phosphorus atom's empty orbital, resulting in a stable bond (Fig. 8b). Therefore, PFAS compounds have a high affinity for this type of bonding, which is why biochar and PFOA molecules can form a strong and stable bond. A combination of covalent bonding (dative interactions) and hydrogen bonds resulting from the functionalization of biochar with H_3PO_4 enhances the adsorbent capacity. Moreover, the carbon matrix's hydrophobic nature and the hydrophobic tail of PFAS molecules enhance PFOA adsorption, which is stabilized by van der Waals forces [78]. PFOA can be effectively removed from water using PBC due to its varied interactions, which enhance adsorption efficiency synergistically.

The use of $ZnCl_2$ in the activation process is critical to improve the biochar structure by increasing porosity and surface area, both of which are crucial for the effective adsorption of contaminants. As a result of catalyst-induced hydrolysis, $ZnCl_2$ causes swelling within the lignocellulosic matrix of biochar, resulting in partial dissolution of cellulose and hemicellulose. By breaking down biomass components, pores are formed, and the number of micro- and mesopores on the surface of the biochar is significantly increased, confirmed by SEM and BET analyses. So, PFOA molecules are more accessible to the biochar, contributing to its increased adsorption capacity.

During activation and pyrolysis, ZnO nanoparticles formed, improving the physical and chemical properties of biochar (As seen in XRD pattern in Fig. 2a). Using ZnO particles as Lewis acid sites, electron-deficient regions can be formed, which interact with species containing electrons. The zinc atoms in ZnO possess empty orbitals that function as electron acceptors, making them ideal for forming dative bonds with electron-donating groups such as the carboxylate (-COO) end of PFOA [77]. A dative bond (Fig. 8b) results from the PFOA molecule donating an electron pair to the zinc empty orbital, resulting in a stable and selective association. This makes ZnBC a promising adsorbent for removing PFOA from water treatment systems.

Chemical and physical interactions occur between PFOA molecules and the chemical functional groups on PBC and ZnBC adsorbents. Many oxygen-containing functional groups on biochar surfaces interact with PFOA, including hydroxyl (-OH), carboxylic (-COOH), ester, epoxide, ketone, aldehyde, and carboxylate groups. The presence of these chemical functional groups has been confirmed by FT-IR and XPS analyses. By hydrogen bonding with the polar head of PFOA, these groups facilitate the retention of PFOA on the surface of the biochar. Further, esterification can occur between certain functional groups on biochar and the carboxylic acid in PFOA, resulting in a more stable covalent bond that contributes to the overall stability of adsorption.

Aromatic rings and aliphatic chains in both PBC and ZnBC introduce non-polar interactions with the fluorinated alkyl tail in PFOA. Due to hydrophobic interactions, the C—F bonds within the PFOA structure create a hydrophobic tail. Bilayers, micelles, and hemimicelles are formed when the PFOA hydrophobic regions interact with the biochar's aromatic and aliphatic moieties. Based on isotherm studies, which indicate a non-uniform distribution of adsorption energies across the biochar surface, this self-aggregation behavior facilitates multilayered adsorption [75].

The adsorption process is enhanced as PFOA molecules cluster and adhere to biochar surfaces due to hydrophobic aggregation. By forming micelle-like structures, multiple PFOA layers adsorb to biochar, increasing its adsorption capacity. As a result of this multilayered adsorption mechanism that is observed in both PBC and ZnBC, these modified biochars are capable of capturing and retaining PFAS compounds with a high level of efficiency. Additionally, hydrogen bonds, esterification, hydrophobic interactions, and van der Waals forces stabilize PFOA adsorbed on biochar and its selective affinity for PFAS compounds.

4. Conclusion

A straightforward technique has been employed in this study to produce a porous carbon adsorbent from abundant canola waste, aimed at removing PFOA from water in both batch and dynamic processes. The effects of H_3PO_4 and $ZnCl_2$ activators on biochar properties were compared to investigate their individual and synergistic impacts. The analysis data confirmed that the activation process enhances the chemical functional groups, surface area, and porosity in the treated biochar adsorbents. The adsorption removal efficiencies of PBC (92 %) and ZnBC (84 %) were significantly higher than those of UBC (5 %). The adsorption behavior of PBC and ZnBC followed the Freundlich isotherm, indicating the presence of a multilayer adsorption process characteristic of modified biochar adsorbents. Additionally, the results showed an excellent fit to the Temkin isotherm, suggesting that PFOA adsorption on these biochar adsorbents also involved electrostatic interaction mechanisms. PBC and ZnBC exhibited high adsorption capacity across a wide pH range, with the highest performance in more acidic conditions.

At room temperature, the adsorption of PFOA by PBC and ZnBC occurred quickly and spontaneously. The results showed that the composition of the solution influenced PFOA adsorption. Therefore, it was important to consider factors such as the possible salting-out effect of anions and the bridging effect of divalent cations in a solution containing adsorbent and PFOA. Efforts were made to evaluate the efficacy of modified adsorbents using fixed-bed column studies under continuous flow conditions, where both treated adsorbents effectively removed PFOA. Future research should focus on scaling up biochar production processes to industrial levels to achieve consistent quality and performance in removing PFAS compounds. In addition, the modified biochar production and application process should be subjected to a life cycle assessment (LCA). A comprehensive understanding of a product's sustainability requires an evaluation of its environmental impact and energy consumption throughout its life cycle. This technology can enhance cost-effectiveness and sustainability through reusability and integration into large-scale treatment systems.

CRediT authorship contribution statement

Malihe Afrooz: Writing – review & editing, Writing – original draft, Validation, Methodology, Investigation, Formal analysis, Conceptualization. **Rahman Zeynali:** Writing – original draft, Software. **Jafar**

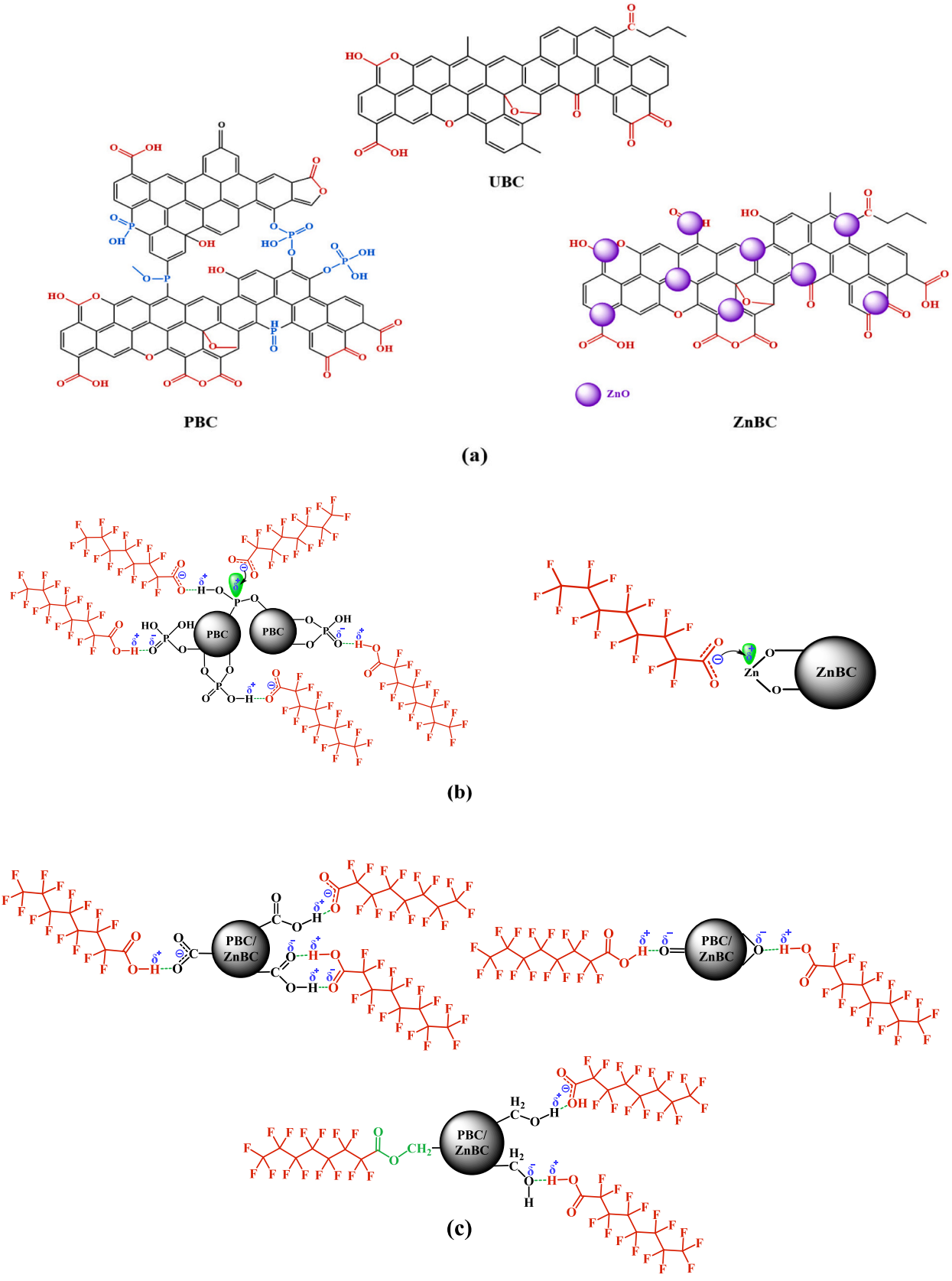

Fig. 8. (a) Structure of UBC, PBC, and ZnBC, (b) formation of dative bonds between phosphorus in PBC (a), zinc in ZnBC (b), and oxygen atoms in PFOA, and (c) various chemical interactions between chemical functional groups containing oxygen of PBC and ZnBC, and PFOA.

Soltan: Writing – review & editing, Validation, Supervision, Conceptualization. **Kerry N. McPhedran:** Writing – review & editing, Writing – original draft, Validation, Supervision, Conceptualization.

Declaration of competing interest

The authors declare that they have no known competing financial interests or personal relationships that could have appeared to influence the work reported in this paper.

Acknowledgement

We express our heartfelt appreciation to the College of Graduate and Postdoctoral Studies at the University of Saskatchewan for awarding M. Afrooz the Dean's Scholarship. Additionally, we extend our gratitude to the Saskatchewan Structural Sciences Centre (SSSC) for providing the analytical facilities essential for this research. The SSSC is funded by the Canada Foundation for Innovation, the Natural Sciences and Engineering Research Council of Canada, and the University of Saskatchewan.

Appendix A. Supplementary data

Supplementary data to this article can be found online at https://doi.org/10.1016/j.jwpe.2024.106586.

Data availability

Data will be made available on request.

References

[1] Y. He, Per- and polyfluoroalkyl substances (PFAS) in China' s groundwater resources: concentration, composition, and human health risk, E3S Web of Conferences 406 (2023), https://doi.org/10.1051/e3sconf/202340602047.
[2] M. Benaafi, A. Bafaqeer, Comprehensive review of global perspectives on per- and Polyfluoroalkyl compounds: occurrence, fate, and remediation in groundwater systems, Water (Switzerland) 16 (11) (2024), https://doi.org/10.3390/w16111583.
[3] B.J. Ruyle, C.P. Thackray, C.M. Butt, D.R. Leblanc, A.K. Tokranov, C.D. Vecitis, E. M. Sunderland, Centurial persistence of forever chemicals at military fire training sites, Environ. Sci. Technol. 57 (21) (2023) 8096–8106, https://doi.org/10.1021/acs.est.3c00675.
[4] Y. Chen, H. Zhang, Y. Liu, J.A. Bowden, T.M. Tolaymat, T.G. Townsend, H.M. Solo-Gabriele, Evaluation of per- and polyfluoroalkyl substances (PFAS) in leachate, gas condensate, stormwater and groundwater at landfills, Chemosphere 318 (January) (2023) 137903, https://doi.org/10.1016/j.chemosphere.2023.137903.
[5] M. Gokgoz, W. Zhang, N. Manage, M. Mbengue, S. Bolyard, J. Chen, Survey on the current leachate treatments of public municipal solid waste landfills and the potential impact of per- and polyfluorinatedalkyl substances in the eastern and northwestern United States, J. Air Waste Manag. Assoc. 73 (8) (2023) 638–648, https://doi.org/10.1080/10962247.2023.2235313.
[6] S.C.E. Leung, P. Shukla, D. Chen, E. Eftekhari, H. An, F. Zare, N. Ghasemi, D. Zhang, N.T. Nguyen, Q. Li, Emerging technologies for PFOS/PFOA degradation and removal: a review, Sci. Total Environ. 827 (2022) 153669, https://doi.org/10.1016/j.scitotenv.2022.153669.
[7] R. Loos, G. Locoro, S. Comero, S. Contini, D. Schwesig, F. Werres, P. Balsaa, O. Gans, S. Weiss, L. Blaha, M. Bolchi, B.M. Gawlik, Pan-European survey on the occurrence of selected polar organic persistent pollutants in ground water, Water Res. 44 (14) (2010) 4115–4126, https://doi.org/10.1016/j.watres.2010.05.032.
[8] R. Mukhopadhyay, B. Sarkar, K.N. Palansooriya, J.Y. Dar, N.S. Bolan, S.J. Parikh, C. Sonne, Y.S. Ok, Natural and engineered clays and clay minerals for the removal of poly- and perfluoroalkyl substances from water: state-of-the-art and future perspectives, Adv. Colloid Interf. Sci. 297 (September) (2021) 102537, https://doi.org/10.1016/j.cis.2021.102537.
[9] D.Q. Zhang, W.L. Zhang, Y.N. Liang, Adsorption of perfluoroalkyl and polyfluoroalkyl substances (PFASs) from aqueous solution - a review, Sci. Total Environ. 694 (2019), https://doi.org/10.1016/j.scitotenv.2019.133606.
[10] A.K. El-Sawaf, S.R. El-Dakkony, M.A. Zayed, A.M. Eldesoky, A.A. Nassar, A. El Shahawy, M.F. Mubarak, Green synthesis and characterization of magnetic gamma alumina nanoparticlesfor copper ions adsorption from synthetic wastewater, Results Eng. 22 (March) (2024) 101971, https://doi.org/10.1016/j.rineng.2024.101971.
[11] M. Trojanowicz, A. Bojanowska-Czajka, I. Bartosiewicz, K. Kulisa, Advanced oxidation/reduction processes treatment for aqueous perfluorooctanoate (PFOA) and perfluorooctanesulfonate (PFOS) – a review of recent advances, Chem. Eng. J. 336 (November 2017) (2018) 170–199, https://doi.org/10.1016/j.cej.2017.10.153.
[12] M. Veciana, J. Bräunig, A. Farhat, M.L. Pype, S. Freguia, G. Carvalho, J. Keller, P. Ledezma, Electrochemical oxidation processes for PFAS removal from contaminated water and wastewater: fundamentals, gaps and opportunities towards practical implementation, J. Hazard. Mater. 434 (April) (2022), https://doi.org/10.1016/j.jhazmat.2022.128886.
[13] D.M. Wanninayake, Comparison of currently available PFAS remediation technologies in water: a review, J. Environ. Manag. 283 (January) (2021) 111977, https://doi.org/10.1016/j.jenvman.2021.111977.
[14] S. Yadav, I. Ibrar, R.A. Al-Juboori, L. Singh, N. Ganbat, T. Kazwini, E. Karbassiyazdi, A.K. Samal, S. Subbiah, A. Altaee, Updated review on emerging technologies for PFAS contaminated water treatment, Chem. Eng. Res. Des. 182 (2022) 667–700, https://doi.org/10.1016/j.cherd.2022.04.009.
[15] F. Liu, J.J. Pignatello, R. Sun, X. Guan, F. Xiao, A comprehensive review of novel adsorbents for per- and polyfluoroalkyl substances in water [review-article], ACS ES and T Water 4 (4) (2024) 1191–1205, https://doi.org/10.1021/acsestwater.3c00569.
[16] C.T. Vu, T. Wu, Recent progress in adsorptive removal of per- and poly-fluoroalkyl substances (PFAS) from water/wastewater, Crit. Rev. Environ. Sci. Technol. 52 (1) (2022) 90–129, https://doi.org/10.1080/10643389.2020.1816125.
[17] M. Zhang, W. Wang, T. Gong, Y. Wu, G. Chen, Cutting-edge technologies and relevant reaction mechanism difference in treatment of long- and short-chain per- and polyfluoroalkyl substances: a review, Chemosphere 354 (March) (2024) 141692, https://doi.org/10.1016/j.chemosphere.2024.141692.
[18] I.M. Militao, F.A. Roddick, R. Bergamasco, L. Fan, Removing PFAS from aquatic systems using natural and renewable material-based adsorbents: a review. *Journal of environmental*, Chem. Eng. 9 (4) (2021), https://doi.org/10.1016/j.jece.2021.105271.
[19] P.S. Pauletto, T.J. Bandosz, Activated carbon versus metal-organic frameworks: a review of their PFAS adsorption performance, J. Hazard. Mater. 425 (November 2021) (2022) 127810, https://doi.org/10.1016/j.jhazmat.2021.127810.
[20] X. Wang, H. Zhang, S. Ham, R. Qiao, Graphene oxide and its derivatives as adsorbents for PFOA molecules [research-article], J. Phys. Chem. B 127 (44) (2023) 9620–9629, https://doi.org/10.1021/acs.jpcb.3c04762.
[21] H.A. Alhashimi, C.B. Aktas, Life cycle environmental and economic performance of biochar compared with activated carbon: a meta-analysis, Resour. Conserv. Recycl. 118 (2017) 13–26.
[22] F. Mushtaq, R. Mat, F.N. Ani, A review on microwave assisted pyrolysis of coal and biomass for fuel production, Renew. Sust. Energ. Rev. 39 (2014) 555–574.
[23] J. Li, J. Dai, G. Liu, H. Zhang, Z. Gao, J. Fu, Y. He, Y. Huang, Biochar from microwave pyrolysis of biomass: a review, Biomass Bioenergy 94 (2016) 228–244.
[24] A. Rehman, M. Park, S.-J. Park, Current progress on the surface chemical modification of carbonaceous materials, Coatings 9 (2) (2019) 103.
[25] L. Leng, Q. Xiong, L. Yang, H. Li, Y. Zhou, W. Zhang, S. Jiang, H. Li, H. Huang, An overview on engineering the surface area and porosity of biochar, Sci. Total Environ. 763 (2021) 144204, https://doi.org/10.1016/j.scitotenv.2020.144204.
[26] T.B. Nguyen, Q.M. Truong, C.W. Chen, R. Doong, an, Chen, W. H., & Dong, C. Di., Mesoporous and adsorption behavior of algal biochar prepared via sequential hydrothermal carbonization and $ZnCl_2$ activation, Bioresour. Technol. 346 (November 2021) (2022) 126351, https://doi.org/10.1016/j.biortech.2021.126351.
[27] Z. Aksu, F. Gönen, Biosorption of phenol by immobilized activated sludge in a continuous packed bed: prediction of breakthrough curves, Process Biochem. 39 (5) (2004) 599–613, https://doi.org/10.1016/S0032-9592(03)00132-8.
[28] Y. Zhang, S. Fan, T. Liu, W. Fu, B. Li, A review of biochar prepared by microwave-assisted pyrolysis of organic wastes, Sustain Energy Technol Assess 50 (January 2021) (2022) 101873, https://doi.org/10.1016/j.seta.2021.101873.
[29] R. Wahi, N.F.Q. Zuhaidi, ain, Yusof, Y., Jamel, J., Kanakaraju, D., & Ngaini, Z., Chemically treated microwave-derived biochar: An overview, Biomass Bioenergy 107 (2017) 411–421, https://doi.org/10.1016/j.biombioe.2017.08.007.
[30] B.R. Patra, A. Mukherjee, S. Nanda, A.K. Dalai, Biochar production, activation and adsorptive applications: a review, Environ. Chem. Lett. 19 (3) (2021) 2237–2259, https://doi.org/10.1007/s10311-020-01165-9.
[31] A. Ateş, The effect of microwave and ultrasound activation on the characteristics of biochar produced from tea waste in the presence of H_3PO_4 and KOH, Biomass Convers. Biorefinery 0123456789 (2021), https://doi.org/10.1007/s13399-021-01838-7.
[32] J. Xu, L. Chen, H. Qu, Y. Jiao, J. Xie, G. Xing, Preparation and characterization of activated carbon from reedy grass leaves by chemical activation with H_3PO_4, Appl. Surf. Sci. 320 (2014) 674–680, https://doi.org/10.1016/j.apsusc.2014.08.178.
[33] O. Oginni, K. Singh, G. Oporto, B. Dawson-Andoh, L. McDonald, E. Sabolsky, Effect of one-step and two-step H_3PO_4 activation on activated carbon characteristics, Biores. Technol. Rep. 8 (July) (2019) 100307, https://doi.org/10.1016/j.biteb.2019.100307.
[34] Z. Ning, B. Xu, W. Zhong, C. Liu, X. Qin, W. Feng, L. Zhu, Preparation of phosphoric acid modified antibiotic mycelial residues biochar: loading of nano zero-valent iron and promotion on biogas production, Bioresour. Technol. 348 (January) (2022) 126801, https://doi.org/10.1016/j.biortech.2022.126801.
[35] L. Yan, Y. Liu, Y. Zhang, S. Liu, C. Wang, W. Chen, C. Liu, Z. Chen, Y. Zhang, $ZnCl_2$ modified biochar derived from aerobic granular sludge for developed microporosity and enhanced adsorption to tetracycline, Bioresour. Technol. 297 (August 2019) (2020) 122381, https://doi.org/10.1016/j.biortech.2019.122381.
[36] M. Hassan, Y. Liu, R. Naidu, S.J. Parikh, J. Du, F. Qi, I.R. Willett, Influences of feedstock sources and pyrolysis temperature on the properties of biochar and functionality as adsorbents: a meta-analysis, Sci. Total Environ. 744 (2020) 140714, https://doi.org/10.1016/j.scitotenv.2020.140714.

[37] A. El Oudiani, Y. Chaabouni, S. Msahli, F. Sakli, Crystal transition from cellulose i to cellulose II in NaOH treated Agave Americana L. fibre, Carbohydr. Polym. 86 (3) (2011) 1221–1229, https://doi.org/10.1016/j.carbpol.2011.06.037.
[38] A.D. French, Idealized powder diffraction patterns for cellulose polymorphs, Cellulose 21 (2) (2014) 885–896, https://doi.org/10.1007/s10570-013-0030-4.
[39] A. Ateş, Investigation of physicochemical and chemical properties of biochar activated with carbonate, nitrate, and borohydride, Biomass Convers. Biorefinery 0123456789 (2024), https://doi.org/10.1007/s13399-024-05323-9.
[40] M. Fathy, M.A. Zayed, Y.M. Moustafa, Synthesis and applications of $CaCO_3$/HPC core–shell composite subject to heavy metals adsorption processes, Heliyon 5 (8) (2019) e02215, https://doi.org/10.1016/j.heliyon.2019.e02215.
[41] M.S. Alam, B. Nahar, M.A. Gafur, G. Seong, M.Z. Hossain, Forced convective heat transfer coefficient measurement of low concentration Nanorods ZnO–ethylene glycol Nanofluids in laminar flow, Nanomaterials 12 (9) (2022), https://doi.org/10.3390/nano12091568.
[42] F. Zhao, R. Shan, W. Li, Y. Zhang, H. Yuan, Y. Chen, Synthesis, characterization, and dye removal of $ZnCl_2$-modified biochar derived from pulp and paper sludge, ACS Omega 6 (50) (2021) 34712–34723, https://doi.org/10.1021/acsomega.1c05142.
[43] C. Guo, R. Hu, W. Liao, Z. Li, L. Sun, D. Shi, Y. Li, C. Chen, Protein-enriched fish "biowaste" converted to three-dimensional porous carbon nano-network for advanced oxygen reduction electrocatalysis, Electrochim. Acta 236 (2017) 228–238, https://doi.org/10.1016/j.electacta.2017.03.169.
[44] O. Pezoti Junior, A.L. Cazetta, R.C. Gomes, É.O. Barizão, I.P.A.F. Souza, A. C. Martins, T. Asefa, V.C. Almeida, Synthesis of $ZnCl_2$-activated carbon from macadamia nut endocarp (Macadamia integrifolia) by microwave-assisted pyrolysis: optimization using RSM and methylene blue adsorption, J. Anal. Appl. Pyrolysis 105 (2014) 166–176, https://doi.org/10.1016/j.jaap.2013.10.015.
[45] S.M. Yakout, G. Sharaf El-Deen, Characterization of activated carbon prepared by phosphoric acid activation of olive stones, Arab. J. Chem. 9 (2016) S1155–S1162, https://doi.org/10.1016/j.arabjc.2011.12.002.
[46] P. Minz, S. Mishra, Jackfruit peel derived $ZnCl_2$-impregnated activated carbon: optimization, characterization, and application in dye removal, Biomass Convers. Biorefinery 0123456789 (2023), https://doi.org/10.1007/s13399-023-04592-0.
[47] E. Yagmur, I.I.G. Inal, Y. Gokce, T.G. Ulusoy Ghobadi, T. Aktar, Z. Aktas, Examination of gas and solid products during the preparation of activated carbon using phosphoric acid, J. Environ. Manag. 228 (September) (2018) 328–335, https://doi.org/10.1016/j.jenvman.2018.09.046.
[48] Y. Wu, L. Qi, G. Chen, A mechanical investigation of perfluorooctane acid adsorption by engineered biochar, J. Clean. Prod. 340 (January) (2022) 130742, https://doi.org/10.1016/j.jclepro.2022.130742.
[49] X. Lei, L. Yao, Q. Lian, X. Zhang, T. Wang, W. Holmes, G. Ding, D.D. Gang, M. E. Zappi, Enhanced adsorption of perfluorooctanoate (PFOA) onto low oxygen content ordered mesoporous carbon (OMC): adsorption behaviors and mechanisms, J. Hazard. Mater. 421 (July 2021) (2022), https://doi.org/10.1016/j.jhazmat.2021.126810.
[50] Y. Zhang, B. Shen, M. Sajjad Ahmad, W. Zhou, R.R. Khalid, M. Ibrahim, A. Bokhari, A three-dimensional active biochar for sintering in steel industry and remove methylene blue by synergistic activation of H_3PO_4 and $ZnCl_2$, Fuel 336 (November 2022) (2023) 127079, https://doi.org/10.1016/j.fuel.2022.127079.
[51] Y. Wu, L. Qi, G. Chen, A mechanical investigation of perfluorooctane acid adsorption by engineered biochar, J. Clean. Prod. 340 (February) (2022) 130742, https://doi.org/10.1016/j.jclepro.2022.130742.
[52] J.H. Kroll, N.M. Donahue, J.L. Jimenez, S.H. Kessler, M.R. Canagaratna, K. R. Wilson, K.E. Altieri, L.R. Mazzoleni, A.S. Wozniak, H. Bluhm, E.R. Mysak, J. D. Smith, C.E. Kolb, D.R. Worsnop, Carbon oxidation state as a metric for describing the chemistry of atmospheric organic aerosol, Nat. Chem. 3 (2) (2011) 133–139, https://doi.org/10.1038/nchem.948.
[53] A.M. Puziy, O.I. Poddubnaya, R.P. Socha, J. Gurgul, M. Wisniewski, XPS and NMR studies of phosphoric acid activated carbons, Carbon 46 (15) (2008) 2113–2123, https://doi.org/10.1016/j.carbon.2008.09.010.
[54] A.H. Ragab, N.F. Gumaah, A.A. El Aziz Elfiky, M.F. Mubarak, Exploring the sustainable elimination of dye using cellulose nanofibrils- vinyl resin based nanofiltration membranes, BMC Chem. 18 (1) (2024) 1–15, https://doi.org/10.1186/s13065-024-01211-5.
[55] K.L. Tan, B.H. Hameed, Insight into the adsorption kinetics models for the removal of contaminants from aqueous solutions, J. Taiwan Inst. Chem. Eng. 74 (2017) 25–48, https://doi.org/10.1016/j.jtice.2017.01.024.
[56] I.M. Militao, F. Roddick, L. Fan, L.C. Zepeda, R. Parthasarathy, R. Bergamasco, PFAS removal from water by adsorption with alginate-encapsulated plant albumin and rice straw-derived biochar. *Journal of water*, Process. Eng. 53 (March) (2023), https://doi.org/10.1016/j.jwpe.2023.103616.
[57] S. Nomura, Y. Kugo, T. Erata, ^{13}C NMR and XRD studies on the enhancement of cellulose II crystallinity with low concentration NaOH post-treatments, Cellulose 27 (7) (2020) 3553–3563, https://doi.org/10.1007/s10570-020-03036-6.
[58] A.K. El-Sawaf, S.R. El-Dakkony, M.A. Zayed, A.M. Eldesoky, A.A. Nassar, A. El Shahawy, M.F. Mubarak, Green synthesis and characterization of magnetic gamma alumina nanoparticlesfor copper ions adsorption from synthetic wastewater. *Results*, Engineering 22 (February) (2024), https://doi.org/10.1016/j.rineng.2024.101971.
[59] W. Chen, X. Zhang, M. Mamadiev, Z. Wang, Sorption of perfluorooctane sulfonate and perfluorooctanoate on polyacrylonitrile fiber-derived activated carbon fibers: in comparison with activated carbon, RSC Adv. 7 (2) (2017) 927–938, https://doi.org/10.1039/c6ra25230c.
[60] I.M. Militao, F. Roddick, L. Fan, L.C. Zepeda, R. Parthasarathy, R. Bergamasco, PFAS removal from water by adsorption with alginate-encapsulated plant albumin and rice straw-derived biochar. *Journal of water*, Process. Eng. 53 (December 2022) (2023), https://doi.org/10.1016/j.jwpe.2023.103616.
[61] B. Saawarn, B. Mahanty, S. Hait, Adsorptive removal of perfluorooctanoic acid from aqueous matrices using peanut husk-derived magnetic biochar: statistical and artificial intelligence approaches, kinetics, isotherm, and thermodynamics, Chemosphere 360 (November 2023) (2024) 142397, https://doi.org/10.1016/j.chemosphere.2024.142397.
[62] S. Chen, C. Qin, T. Wang, F. Chen, X. Li, H. Hou, M. Zhou, Study on the adsorption of dyestuffs with different properties by sludge-rice husk biochar: adsorption capacity, isotherm, kinetic, thermodynamics and mechanism, J. Mol. Liq. 285 (2019) 62–74, https://doi.org/10.1016/j.molliq.2019.04.035.
[63] J. Zang, T. Wu, J. Yang, Z. Xie, S. Fan, J. Tang, Sorption behavior of perfluorooctane sulfonate on hydrous ferric oxide from aqueous solution, Desalin. Water Treat. 226 (2021) 197–207, https://doi.org/10.5004/dwt.2021.27270.
[64] E.C. Lima, A.A. Gomes, H.N. Tran, Comparison of the nonlinear and linear forms of the van't Hoff equation for calculation of adsorption thermodynamic parameters (ΔS° and ΔH°), J. Mol. Liq. 311 (2020) 113315, https://doi.org/10.1016/j.molliq.2020.113315.
[65] P.N. Omo-Okoro, C.J. Curtis, P. Karásková, L. Melymuk, O.A. Oyewo, J. O. Okonkwo, Kinetics, isotherm, and thermodynamic studies of the adsorption mechanism of PFOS and PFOA using inactivated and chemically activated maize tassel, Water Air Soil Pollut. 231 (9) (2020), https://doi.org/10.1007/s11270-020-04852-z.
[66] S. Hong, C. Wen, J. He, F. Gan, Y.S. Ho, Adsorption thermodynamics of methylene blue onto bentonite, J. Hazard. Mater. 167 (1–3) (2009) 630–633, https://doi.org/10.1016/j.jhazmat.2009.01.014.
[67] O.A. Salawu, Z. Han, A.S. Adeleye, Shrimp waste-derived porous carbon adsorbent: performance, mechanism, and application of machine learning, J. Hazard. Mater. 437 (February) (2022) 129266, https://doi.org/10.1016/j.jhazmat.2022.129266.
[68] J.M. Jian, C. Zhang, F. Wang, X. Lu, F. Wang, E.Y. Zeng, Effect of solution chemistry and aggregation on adsorption of perfluorooctanesulphonate (PFOS)to nano-sized alumina, Environ. Pollut. 251 (2019) 425–433, https://doi.org/10.1016/j.envpol.2019.05.025.
[69] K.-U. Goss, The p K a values of PFOA and other highly fluorinated carboxylic acids, Environ. Sci. Technol. 42 (2008) 456–458, https://doi.org/10.1021/es8011904.
[70] F. Wang, K. Shih, Adsorption of perfluorooctanesulfonate (PFOS) and perfluorooctanoate (PFOA) on alumina: influence of solution pH and cations, Water Res. 45 (9) (2011) 2925–2930, https://doi.org/10.1016/j.watres.2011.03.007.
[71] J. Jeon, K. Kannan, H.K. Lim, H.B. Moon, J.S. Ra, S.D. Kim, Bioaccumulation of perfluorochemicals in pacific oyster under different salinity gradients, Environ. Sci. Technol. 44 (7) (2010) 2695–2701, https://doi.org/10.1021/es100151r.
[72] Q. Yu, R. Zhang, S. Deng, J. Huang, G. Yu, Sorption of perfluorooctane sulfonate and perfluorooctanoate on activated carbons and resin: kinetic and isotherm study, Water Res. 43 (4) (2009) 1150–1158, https://doi.org/10.1016/j.watres.2008.12.001.
[73] L.A. Ramírez-Montoya, V. Hernández-Montoya, A. Bonilla-Petriciolet, M. A. Montes-Morán, R. Tovar-Gómez, M.R. Moreno-Virgen, Preparation, characterization and analyses of carbons with natural and induced calcium compounds for the adsorption of fluoride, J. Anal. Appl. Pyrolysis 105 (2014) 75–82, https://doi.org/10.1016/j.jaap.2013.10.005.
[74] V.J. Inglezakis, M. Balsamo, F. Montagnaro, Liquid-solid mass transfer in adsorption systems - An overlooked resistance? Ind. Eng. Chem. Res. 59 (50) (2020) 22007–22016, https://doi.org/10.1021/acs.iecr.0c05032.
[75] Z. Du, S. Deng, Y. Bei, Q. Huang, B. Wang, J. Huang, G. Yu, Adsorption behavior and mechanism of perfluorinated compounds on various adsorbents-a review, J. Hazard. Mater. 274 (2014) 443–454, https://doi.org/10.1016/j.jhazmat.2014.04.038.
[76] H. Yang, P. Chen, W. Chen, K. Li, M. Xia, H. Xiao, X. Chen, Y. Chen, X. Wang, H. Chen, Insight into the formation mechanism of N, P co-doped mesoporous biochar from H_3PO_4 activation and NH_3 modification of biomass, Fuel Process. Technol. 230 (February) (2022) 107215, https://doi.org/10.1016/j.fuproc.2022.107215.
[77] M.J. Valero-Romero, F.J. García-Mateos, J. Rodríguez-Mirasol, T. Cordero, Role of surface phosphorus complexes on the oxidation of porous carbons, Fuel Process. Technol. 157 (2017) 116–126, https://doi.org/10.1016/j.fuproc.2016.11.014.
[78] G. He, G. Pan, M. Zhang, Assembling structures and dynamics properties of perfluorooctane sulfonate (PFOS) at water-titanium oxide interfaces, J. Colloid Interface Sci. 405 (2013) 189–194, https://doi.org/10.1016/j.jcis.2013.05.003.
[79] C. Pronyk, G. Mazza, Fractionation of triticale, wheat, barley, oats, canola, and mustard straws for the production of carbohydrates and lignins, Bioresour. Technol. ISSN: 0960-8524 106 (124) (2012) 117, https://doi.org/10.1016/j.biortech.2011.11.071.
[80] J.M. Rosas, J. Bedia, J. Rodríguez-Mirasol, T. Cordero, Preparation of hemp-derived activated carbon monoliths: Adsorption of water vapor, Ind. Eng. Chem. Res. 47 (4) (2008) 1288–1296, https://doi.org/10.1021/ie070924w.